2. EXPLANATORY NOTES[1]

Shipboard Scientific Party[2]

INTRODUCTION

In this chapter, we have assembled information that will help the reader understand the basis for our preliminary conclusions and also help the interested investigator select samples for further analysis. This information concerns only shipboard operations and analyses described in the site reports in the *Initial Reports* volume of this Leg 167 *Proceedings of the Ocean Drilling Program.* Methods used by various investigators for shore-based analyses of Leg 167 data will be detailed in the individual scientific contributions published in the *Scientific Results* volume.

Authorship of Site Chapters

The separate sections of the site chapters were written by the following shipboard scientists (authors are listed in alphabetical order; no seniority is implied):

Principal results: Koizumi, Lyle, Richter
Background and objectives: Lyle
Operations: McGrath, Richter
Lithostratigraphy: Behl, Desmet, Hovan, Mossman, Pike, Tada, Thurow
Biostratigraphy: Caulet, Fornaciari, Kennett, Machain-Castillo, Maruyama, Rozo-Vera
Paleomagnetism: Hayashida, Heider
Composite depth and sedimentation rates: Janecek, Ravelo
Inorganic geochemistry: Delaney
Organic geochemistry: Stax, Yamamoto
Physical properties: Bodén, Hood, Janik, Lund, Merrill, Thurow
Downhole measurements: deMenocal, Ravelo
Summary: Lyle
Appendix (Barrel sheets, VCDs, etc.): Shipboard Scientific Party

Summary core descriptions ("barrel sheets") and photographs of each core are included in a section called "Cores" following the text of the site chapters.

Use of "Ma" vs. "m.y."

1. *Ma* is equivalent to and replaces m.y.B.P. (million years Before Present), for example, 35–40 Ma.
2. *m.y.* is used in sentences such as "... for 5 m.y. in the early Miocene."

Drilling Characteristics

Information concerning sedimentary stratification in uncored or unrecovered intervals may be inferred from seismic data, wireline-logging results, and from an examination of the behavior of the drill string, as observed and recorded on the drilling platform. Typically, the harder a layer is, the slower and more difficult it is to penetrate. A number of other factors may determine the rate of penetration, so it is not always possible to relate the drilling time directly to the hardness of the layers. Bit weight and revolutions per minute, recorded on the drilling recorder, also influence the penetration rate.

Drilling Deformation

When cores are split, many show signs of significant sediment disturbance, including the concave-downward appearance of originally horizontal bands, haphazard mixing of lumps of different lithologies (mainly at the tops of cores), and the near-fluid state of some sediments recovered from tens to hundreds of meters below the seafloor. Core deformation probably occurs during cutting, retrieval (with accompanying changes in pressure and temperature), and core handling on deck.

Shipboard Scientific Procedures

Numbering of Sites, Holes, Cores, and Samples

ODP drill sites are numbered consecutively and refer to one or more holes drilled while the ship was positioned over one acoustic beacon. Multiple holes may be drilled at a single site by pulling the drill pipe above the seafloor (out of the hole), moving the ship some distance from the previous hole, and then drilling another hole.

For all ODP drill sites, a letter suffix distinguishes each hole drilled at the same site. The first hole drilled is assigned the site number modified by the suffix "A," the second hole takes the site number and suffix "B," and so forth. Note that this procedure differs slightly from that used by DSDP (Sites 1 through 624), but prevents ambiguity between site- and hole-number designations. It is important to distinguish among holes drilled at a site, because recovered sediments or rocks from different holes usually do not come from exactly equivalent positions in the stratigraphic column.

The cored interval is measured in meters below seafloor (mbsf). The depth interval assigned to an individual core begins with the depth below the seafloor that the coring operation began and extends to the depth that the coring operation ended (see Fig. 1). Each cored interval is generally 9.5 m long, which is the length of a core barrel. Coring intervals may be shorter and may not necessarily be adjacent if separated by drilled intervals. In soft sediments, the drill string can be "washed ahead" with the core barrel in place, without recovering sediments. This is achieved by pumping water down the pipe at high pressure to wash the sediment out of the way of the bit and up the space between the drill pipe and the wall of the hole. If thin, hard, rock layers are present, then it is possible to get "spotty" sampling of these resistant layers within the washed interval and thus to have a cored interval greater than 9.5 m. When drilling hard rock, a center bit may replace the core barrel if it is necessary to drill without core recovery.

Cores taken from a hole are numbered serially from the top of the hole downward. Core numbers and their associated cored intervals in meters below seafloor ideally are unique in a given hole; however, this may not be true if an interval is cored twice, if the borehole wall caves in, or other hole problems occur. Full recovery for a single core is 9.5 m of rock or sediment contained in a plastic liner (6.6-cm internal diameter) plus about 0.2 m (without a plastic liner) in the core

[1]Lyle, M., Koizumi, I., Richter, C., et al., 1997. *Proc. ODP, Init. Repts.*, 167: College Station, TX (Ocean Drilling Program).
[2]Shipboard Scientific Party is given in the list preceding the Table of Contents.

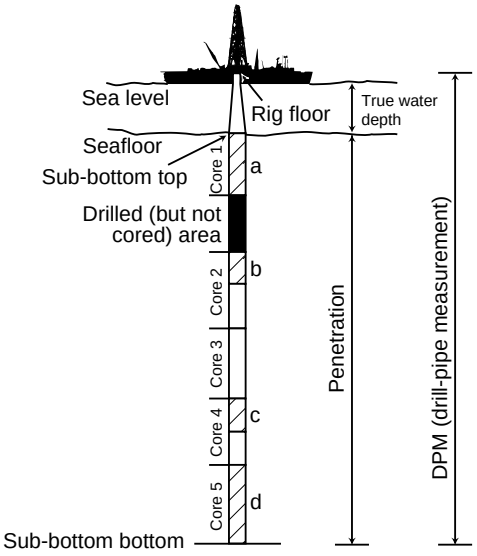

Bottom felt: distance from rig floor to seafloor
Total depth: distance from rig floor to bottom of hole (sub-bottom bottom)
Penetration: distance from seafloor to bottom of hole (sub-bottom bottom)
Number of cores: total of all cores recorded, including cores with no recovery
Total length of cored section: distance from sub-bottom top to sub-bottom bottom minus drilled (but not cored) areas in between
Total core recovered: total from adding a, b, c, and d in diagram
Core recovery (%): equals total core recovered divided by total length of cored section times 100

Figure 1. Coring and depth intervals.

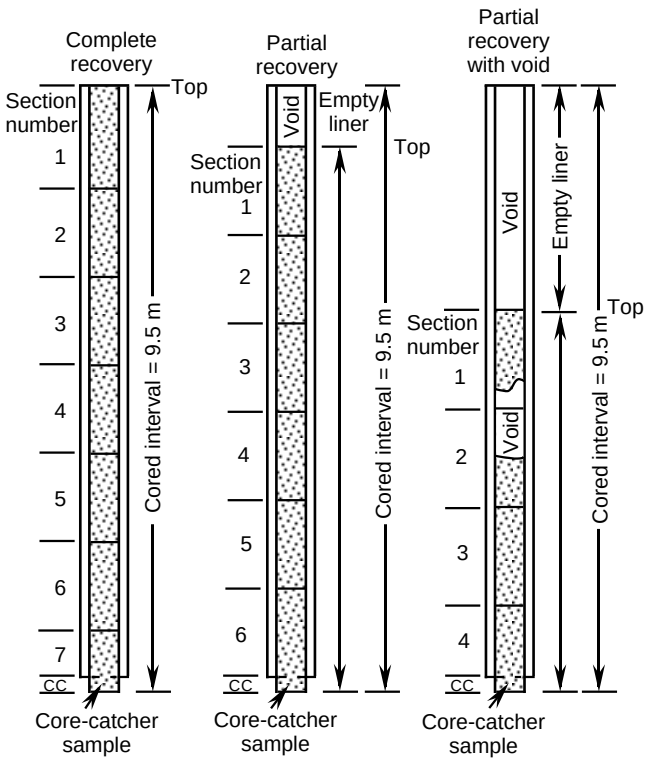

Figure 2. Examples of numbered core sections.

catcher (Fig. 2). The core catcher is a device at the bottom of the core barrel that prevents the core from sliding out when the barrel is being retrieved from the hole. In many APC/XCB cores, recovery exceeds the 9.5-m theoretical maximum by as much as 0.60 m. The cause of this expansion is not fully understood. The recovered core in its liner is divided into 1.5-m sections that are numbered serially from the top (Fig. 2). When full recovery is obtained, the sections are numbered from 1 through 7, with the last section generally being shorter than 1.5 m. Rarely, a core may require more than seven sections; this is usually the result of gas expansion having caused voids within some sections. When less than full recovery is obtained, as many sections as are needed to accommodate the length of the core will be recovered; for example, 4 m of core would be divided into two 1.5-m sections and a 1-m section. If cores are fragmented (recovery less than 100%), sections are numbered serially and intervening sections are noted as void, whether shipboard scientists believe that the fragments were contiguous in situ or not. In rare cases, a section less than 1.5 m may be cut to preserve features of interest. Sections less than 1.5 m in length are also sometimes cut when the core liner is severely damaged.

By convention, material recovered from the core catcher is placed immediately below the last section when the core is described and is labeled core catcher (CC); in sedimentary cores, it is treated as a separate section. The core catcher is assigned the depth of the top of the cored interval in cases where material is only recovered in the core catcher (this convention differs from that used in the early days of deep-sea drilling), although information from the driller or other sources may indicate from what depth it was actually recovered.

When the recovered core is shorter than the cored interval, the top of the core is equated with the top of the cored interval by convention, to achieve consistency when handling analytical data derived from the cores. Samples removed from the cores are designated by distance, measured in centimeters from the top of the section to the top and bottom of each sample removed from that section. A complete identification number for a sample consists of the following information: leg, site, hole, core number, core type, section number, piece number (for hard rock), and interval in centimeters, measured from the top of the section. For example, a sample identification of "167-1010A-15H-6, 10–12 cm" would be interpreted as representing a sample removed from the interval between 10 and 12 cm below the top of Section 6, Core 15 (H designates that this core was taken by the advanced hydraulic piston corer) of Hole 1010A during Leg 167. A computer routine was available to calculate depth in mbsf from any correctly formulated ODP sample designation; this avoids inconsistencies that frequently arise on those occasions where some sections were cut to non-standard lengths. Although depth in mbsf is an invaluable convention, it is not ideal especially for high-resolution work; for composite depths see below.

All ODP core and sample identifiers indicate core type. The following abbreviations are used: H = hydraulic piston core (HPC; also referred to as APC, or advanced hydraulic piston core); X = extended core barrel (XCB); B = drill-bit recovery; C = center-bit recovery; I = in situ water sample; S = sidewall sample; N = motor-driven core barrel (MDCB); W = wash-core recovery; and M = miscellaneous material. APC, XCB, and MDCB cores were cut during Leg 167.

Core Handling

As soon as a core was retrieved on deck, a sample taken from the core catcher was given to the paleontological laboratory for an initial age assessment. Special care was taken in transferring the core from the drill floor to a long horizontal rack on a catwalk near the core laboratory so that the core did not bend or twist excessively. The core was capped immediately, and gas samples were taken by piercing the

core liner and withdrawing gas into a vacuum tube. Voids within the core were sought as sites for gas sampling. Some of the gas samples were stored for shore-based study, but others were analyzed immediately as part of the shipboard safety and pollution-prevention program. Next, the core was marked into section lengths of 150 cm, each section was labeled, and the core was cut into sections. Interstitial water (IW) and whole-round physical properties (PP) samples were also taken at this time. In addition, some headspace gas samples were taken from the end of cut sections on the catwalk and sealed in glass vials for light hydrocarbon analysis. Afterward, each section was sealed at the top and bottom by gluing on color-coded plastic caps: blue to identify the top of a section and clear for its bottom. A yellow cap was placed on the section ends from which a whole-round sample was removed. The caps were usually attached to the liner by coating the end liner and the inside rim of the cap with acetone and then attaching the caps to the liners.

Next, the cores were carried into the laboratory, where the sections were labeled with an engraver to mark the complete designation of the section permanently. The length of the core in each section and the core-catcher sample were measured to the nearest centimeter. This information was logged into the shipboard CORELOG database program.

Whole-round sections from APC and XCB cores normally were run through the multisensor track (MST). The MST includes the gamma-ray attenuation porosity evaluator (GRAPE), the *P*-wave logger, natural gamma-ray emission sensor, and a volume magnetic susceptibility meter. The core-catcher sample is not run through the MST. Prior to MST analysis, the temperature of each core was measured. After the core had equilibrated to room temperature (approximately 3 hr), soft sediments were measured for thermal conductivity before being split. Cores were split lengthwise into working and archive halves. Softer cores were split with a wire from bottom to top so that the soupy intervals that were sometimes present at the top of Section 1 would not be drawn down the section. Harder cores were split using a diamond saw.

After splitting, working and archive halves of each section were designated, and the archive halves were described visually. Smear slides were made from samples taken from the archive half. Next, the archive half of the core was run through the Oregon State University color reflectance scanner, the ODP digital color scanner, and the cryogenic magnetometer. Finally, the cores were photographed with both black-and-white and color film, a whole core at a time. Close-up photographs (black-and-white) were taken of particular features, as requested by individual scientists, for illustrations in the summary of each site.

The working half of the core was measured first for sonic velocity. After physical properties sampling, the working half was sampled for reconnaissance-level and low-resolution shipboard and shore-based laboratory studies. Most sampling for detailed high-resolution paleoceanographic and paleoclimatic studies was deferred until after the cruise to optimize the sampling with the stratigraphic information from biostratigraphy, magnetostratigraphy, and lithologic correlations.

Each sample taken either for shipboard or shore-based analysis was logged into the sampling database program by the location and the name of the investigator receiving the sample. Records of all of the samples removed are kept by the curator at ODP headquarters. The extracted samples were sealed in plastic vials or bags and labeled. Samples were routinely taken for shipboard physical property analysis and for calcium carbonate (coulometric) and organic carbon (CNS elemental) analyses; these data are reported in the site chapters and on CD-ROM.

Both halves of the core were placed into labeled plastic tubes, which were then sealed and transferred to cold-storage space aboard the drilling vessel. At the end of the leg, the cores were transferred from the ship in refrigerated air-freight containers to cold storage.

LITHOSTRATIGRAPHY

Sediment Core Description

Preparation of Surfaces of Core Halves

The standard method of splitting cores by pulling a wire lengthwise through the center tends to smear the cut surface of soft sediments and obscure fine details of lithology and sedimentary structure. For Leg 167, the archive halves of cores were carefully scraped with a stainless steel or glass scraper to clean the surface for sedimentologic examination and video imaging. Scraping was done parallel to bedding to prevent cross-stratigraphic contamination.

Barrel Sheets

Detailed sedimentologic observations and descriptions were recorded by hand on sediment core description forms ("barrel sheets") or section-by-section on handwritten Visual Core Description Sheets. These observations are synthesized for each core in the computer-formatted sediment core description forms ("barrel sheets") (Fig. 3). Exceptions to the standard ODP conventions adopted by the Leg 167 Scientific Party are described below.

Graphic Lithology Column

Leg 167 used a slightly expanded version of the lithological classification scheme of Mazzullo et al. (1988). The classification adopted is outlined in the "Sediment Classification" section of this chapter. Sediment type is represented graphically on the core description forms using the symbols illustrated in Figure 4.

In the "Graphic Lithology" column, a maximum of three different lithologies (for interbedded sediments) or three different components (for mixed sediments) can be represented within the same core interval. Minor lithologies present as thin interbeds within the major lithology are shown by a dashed vertical line dividing the lithologies. Components present as minor fractions of the main lithology are shown by a continuous vertical line. Percentages are rounded to the nearest 10% and lithologies that constitute less than 10% of the core are not shown, but are listed in the "Lithologic Description" section. Only lithologic units that are 20 cm or greater in thickness can be accurately portrayed in this column.

Chronostratigraphy

The chronostratigraphic unit, based on paleontological results, is shown in the "Age" column. Zonations and ages used during Leg 167 are presented in the "Biostratigraphy" section, this chapter.

Sedimentary Structures

The locations and types of sedimentary structures visible on the prepared surface of the archive half of cores are shown in the "Structure" column of the core description form. The column is divided into three vertical areas for symbols (Fig. 3). The symbols on the left side of the "Structure" column indicate the bedding characteristics (including color banding) of the sediment. We followed a slightly amended version of McKee and Weir (1953) to distinguish thicknesses of bedding units, whether identified by composition, texture, or color. Stratigraphic units are very thick bedded (or banded) if >100 cm in thickness, thick bedded (30–100 cm), medium bedded (10–30 cm), thin bedded (1–10 cm), and laminated if <1 cm in thickness. The abundance of visually detectable burrows is shown in the central portion of the "Structure" column of the barrel sheet in the conventional manner (none, rare, common, abundant). The symbols on the right hand side of the "Structure" column indicate the location of individ-

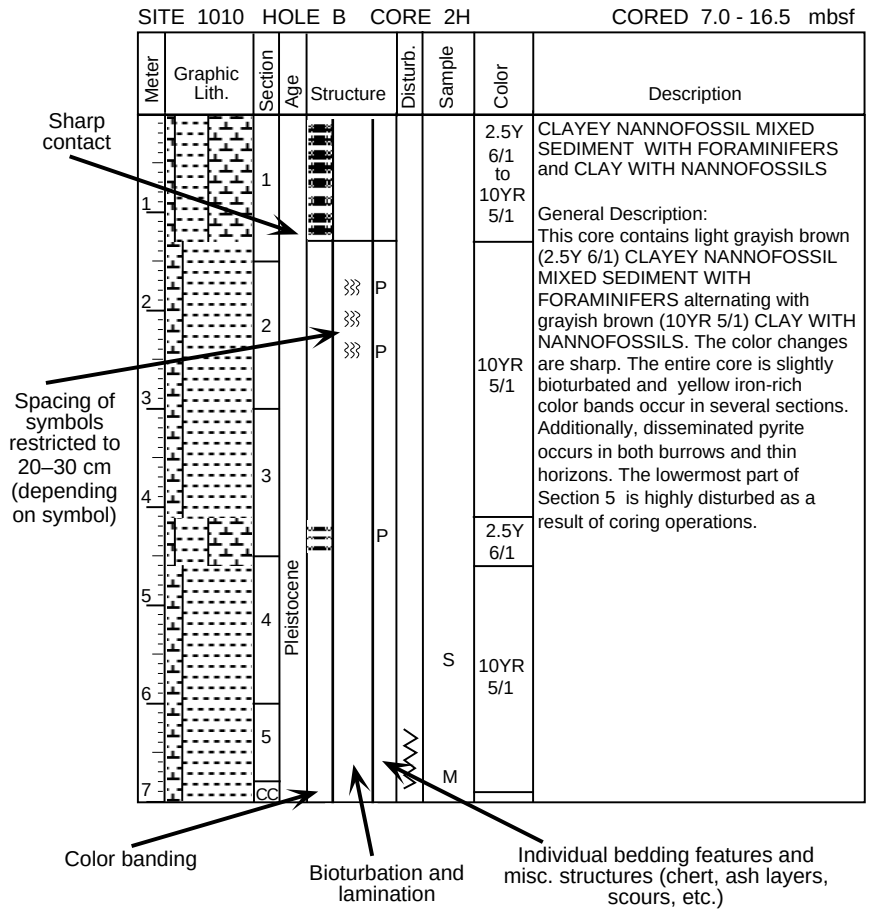

Figure 3. Example of core description sheet form (barrel sheet) used for sediments and sedimentary rocks on Leg 167.

ual bedding features and any other sedimentary features such as nodules, scours, ash layers, ripple lamination, or shell fragments. The symbols used to designate the structures found in Leg 167 cores are shown in Figure 5.

Sediment Disturbance

Drilling-related sediment disturbance that persists over intervals of approximately 20 cm or more is recorded in the "Disturbance" column using the symbols shown in Figure 5. The degree of drilling disturbance is described for soft and firm sediments using the following categories:

1. Slightly disturbed: bedding contacts are slightly deformed.
2. Moderately disturbed: bedding contacts have undergone extreme bowing.
3. Highly disturbed: bedding is completely deformed as flow-in, coring/drilling slough, and other soft sediment stretching and/or compressional shearing structures attributed to the coring/drilling.
4. Soupy: intervals are water-saturated and have lost all aspects of original bedding.

The degree of fracturing in indurated sediments and igneous rocks is described using the following categories:

1. Slightly fractured: core pieces in place and broken.
2. Moderately fractured: core pieces are in place or partly displaced, and original orientation is preserved or recognizable (drilling slurry may surround fragments, that is, drilling/coring "biscuits" are evident).
3. Highly fractured: core pieces are probably in correct stratigraphic sequence (although they may not represent the entire sequence), but original orientation is lost.
4. Drilling breccia: the core is crushed and broken into many small and angular pieces, with original orientation and stratigraphic position lost; often drilling breccia is completely mixed with drilling slurry.

Samples

The positions of samples taken from each core for analysis are indicated by letters in the "Sample" column of the core description form as follows: S (smear slide), M (micropaleontology), I (interstitial water), and D (X-ray diffraction).

Color

Color, hue, and chroma attributes were determined visually by comparison with Munsell soil-color and rock-color charts after the core-half surface was cleaned with a stainless steel or glass scraper. These values were occasionally confirmed by the ODP Digital Color Imaging System; color was also measured by two prototype electronic systems (see "Physical Properties" section, this chapter). Observations were made of the damp core surface as soon as possible after the core was split. It should be noted with caution that many surficial oxidation reactions are completed within seconds after splitting organic-rich cores of reduced sediment, and the surface colors documented

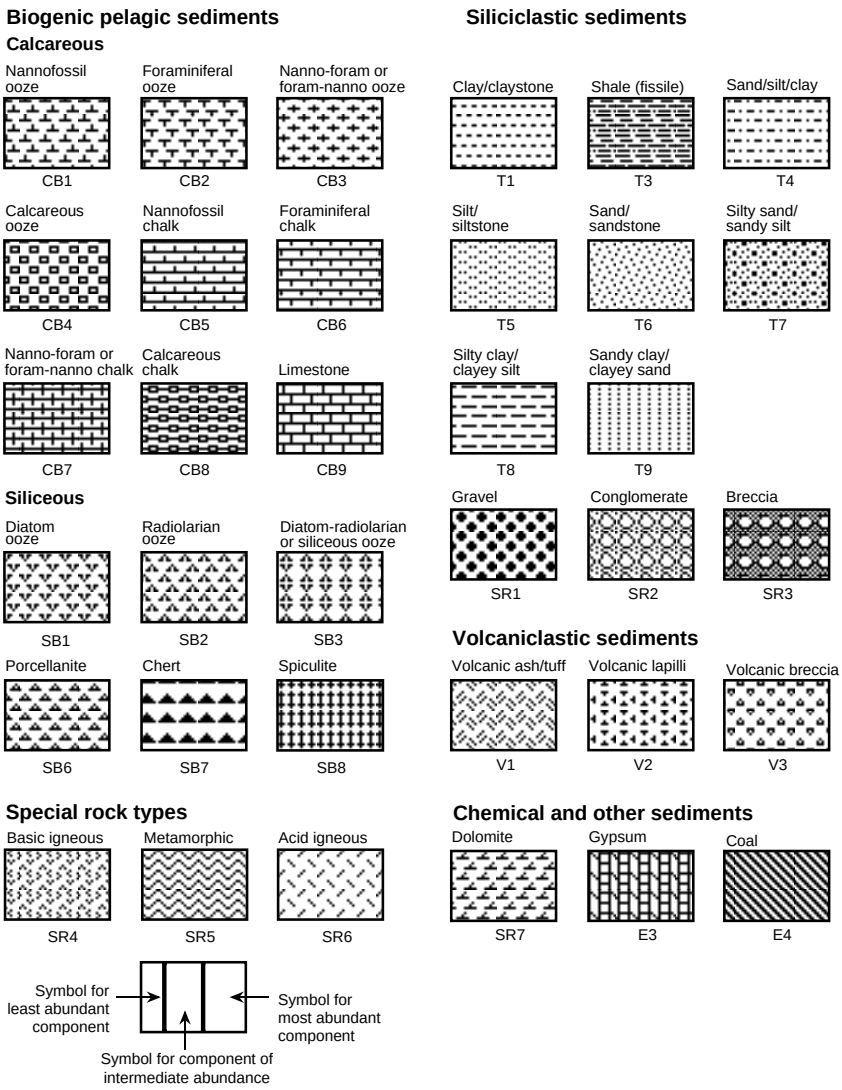

Figure 4. Key to symbols used in the "Graphic Lithology" column on the core description sheets.

here are not necessarily the same as the pristine, unoxidized sediment prior to exposure to atmospheric oxygen or as the stable equilibrium colors reached after complete surface oxidation.

Lithologic Description Text

The lithologic description that appears on each core description form (barrel sheet) consists of three parts: (1) a heading that lists all the major sediment lithologies observed in the core; (2) a heading for minor lithologies, and (3) a more detailed description of these sediments, including location in the core of significant features. Descriptions and locations of thin, interbedded, or minor lithologies are included in the text.

Smear Slides

Smear-slide analysis data tables are included on the CD-ROM, back pocket, this volume. These tables include information about the sample location, whether the sample represents a dominant (D) or a minor (M) lithology in the core, and the estimated percentages of sand, silt, and clay, together with all identified components. Note that smear-slide analyses tend to underestimate the abundance of sand-sized grains (e.g., foraminifers, radiolarians, and siliciclastic sand), because these are difficult to incorporate into the smear. At the same time, clay-sized fine biosilica, being transparent and isotropic, is very difficult to quantify.

Sediment Classification

Classification of Sediments and Sedimentary Rocks

The sediment classification used during Leg 167 closely follows that proposed by Mazzullo et al. (1988) for the Ocean Drilling Program. The classification scheme is descriptive rather than genetic and is based predominantly on texture and composition. Classification depended entirely on data collected on board the *JOIDES Resolution*, which included smear-slide analyses, visual core descriptions, coulometrically determined calcium carbonate, X-ray diffraction, and grain-size estimates obtained by microscope observation.

The only modification of the standard ODP classification scheme is a clarification of the distinction between porcellanite and chert, which is outlined below.

Classes of Granular Sediments

Variations in the relative proportions of different grain types define five major classes of granular sediments: pelagic, neritic, siliciclastic, volcaniclastic, and mixed (Fig. 6). Pelagic grains are the skeletal remains of open marine siliceous and calcareous microbiota

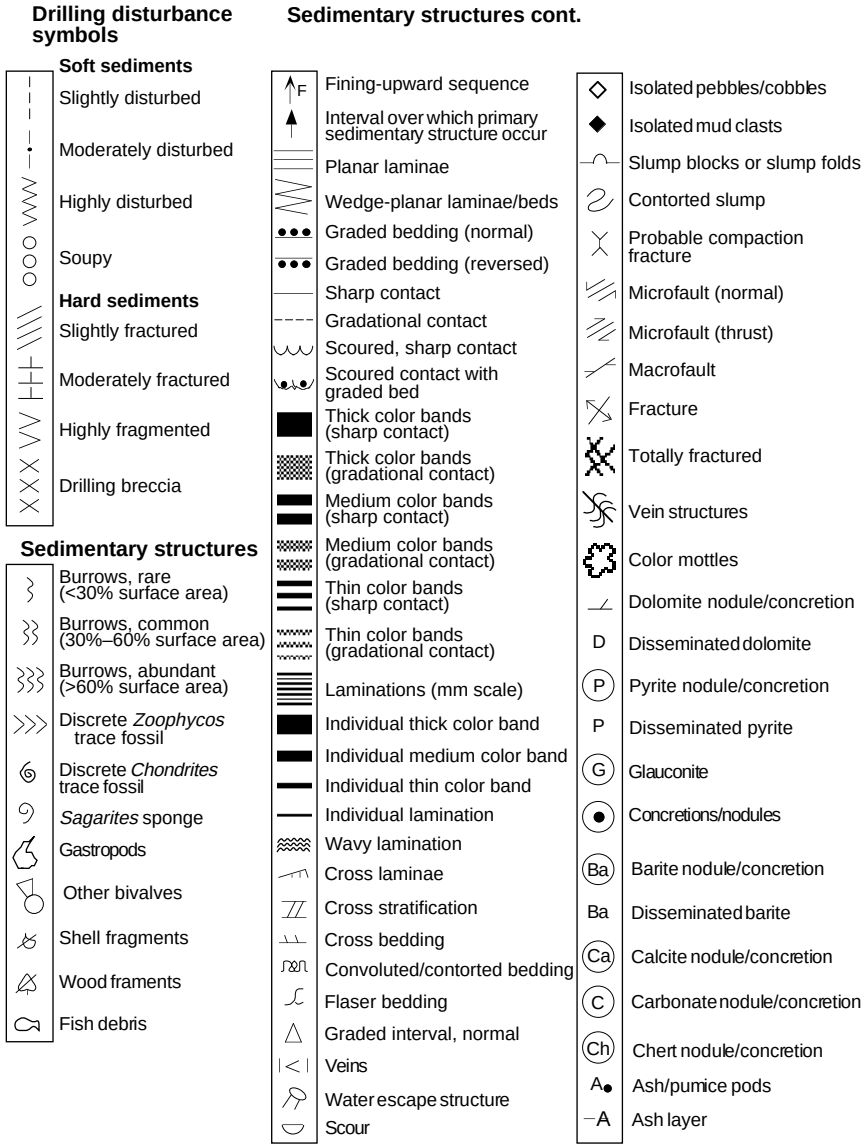

Figure 5. Key to symbols used in the "Structures" column on the core description sheets.

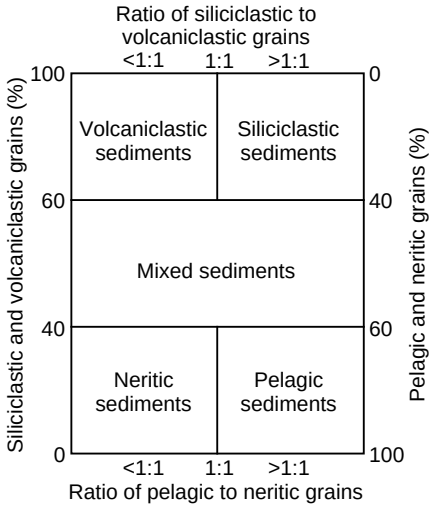

Figure 6. Diagram showing classes of granular sediment (after Mazzullo et al., 1988).

(e.g., radiolarians, diatoms, planktonic foraminifers, nannofossils) and associated organisms. Neritic grains include calcareous grains and skeletal remains (e.g., bioclasts, shallow-water benthic foraminifers, peloids) of non-pelagic origin. Siliciclastic grains are mineral and rock fragments derived from plutonic, sedimentary, and metamorphic rocks. Volcaniclastic grains include those of pyroclastic (direct products of magma degassing) and epiclastic origin (detritus derived from erosion of volcanic rocks).

1. Pelagic sediments are composed of >60% pelagic and neritic grains and <40% siliciclastic and volcaniclastic grains. They also contain a higher proportion of pelagic than neritic grains.
2. Neritic sediments are composed of >60% neritic and pelagic grains and <40% siliciclastic and volcaniclastic grains. They contain a higher proportion of neritic than pelagic grains.
3. Siliciclastic sediments are composed of >60% siliciclastic and volcaniclastic grains and <40% pelagic and neritic grains. They contain a higher proportion of siliciclastic than volcaniclastic grains.
4. Volcaniclastic sediments are composed of >60% siliciclastic and volcaniclastic grains and <40% pelagic and calciclastic

Table 1. Outline of granular-sediment classification scheme.

Sediment class	Major modifiers	Principal name	Minor modifiers
Pelagic sediment	1. Composition of pelagic and neritic grains present in major amounts 2. Texture of clastic grains present in major amounts	1. Ooze 2. Chalk 3. Limestone 4. Radiolarite 5. Diatomite 6. Spiculite 7. Porcellanite 8. Chert	1. Composition of pelagic and neritic grains present in minor amounts 2. Texture of clastic grains present in minor amounts
Neritic sediment	1. Composition of neritic and pelagic grains present in major amounts 2. Texture of clastic grains present in major amounts	1. Boundstone 2. Grainstone 3. Packstone 4. Wackestone 5. Mudstone 6. Floatstone 7. Rudstone	1. Composition of neritic and pelagic grains present in minor amounts 2. Texture of clastic grains present in minor amounts
Siliciclastic sediment	1. Composition of all grains present in major amounts 2. Grain fabric (gravels only) 3. Sediment color (optional) 4. Grain shape (optional)	1. Gravel 2. Sand 3. Silt 4. Clay	1. Composition of all grains present in minor amounts 2. Texture and composition of siliciclastic grains present as matrix (for coarse-grained clastic sediments)
Volcaniclastic sediment	1. Composition of all volcaniclasts present in major amounts 2. Composition of all pelagic and neritic grains present in major amounts 3. Texture of siliciclastic grains present in major amounts	1. Breccia 2. Lapilli 3. Ash/tuff	1. Composition of all volcaniclasts present in minor amounts 2. Composition of all pelagic and neritic grains present in minor amounts 3. Texture of siliciclastic grains present in minor amounts
Mixed sediments	1. Composition of neritic and pelagic grains present in major amounts 2. Texture of clastic grains present in major amounts	1. Mixed sediments	1. Composition of neritic and pelagic grains present in minor amounts 2. Texture of clastic grains present in minor amounts

Note: Table modified from Mazzullo et al. (1988).

grains. They contain a higher proportion of volcaniclastic than siliciclastic grains.

5. Mixed sediments are composed of 40%–60% siliciclastic and volcaniclastic grains and 40%–60% pelagic and neritic grains.

Classification of Granular Sediment

A granular sediment is classified by designating a principal name with additional major and minor modifiers (Mazzullo et al., 1988). The principal name of a granular sediment defines its granular-sediment class (Table 1). The major and minor modifiers describe the texture, composition, fabric, or roundness of the grains themselves.

Major and Minor Modifiers

The principal name of a granular-sediment class is preceded by major modifiers and followed by minor modifiers (preceded by "with") that describe the lithology of the granular sediment in greater detail (Table 1). Major and minor modifiers are used to describe composition and grain size of particles present in major (>25%) and minor (10%–25%) proportions. In addition, major modifiers can be used to describe degree of lithification, grain fabric, grain shape, and sediment color. Modifiers are always listed in order of increasing abundance. For a complete discussion of the nomenclature for major and minor modifiers, see Mazzullo et al. (1988).

Classification of Diagenetic Siliceous Rocks

Chert and porcellanite are two types of hard, lithified siliceous rocks recovered during Leg 167. Chert and porcellanite are used by the sedimentologists as field terms based on easily observable physical properties; these names are *not* strictly dependent on mineralogy. Cherts and porcellanites can each be composed of either diagenetic quartz (microcrystalline, cryptocrystalline, or chalcedonic varieties) or opal-CT (opal-cristobalite/tridymite). Chert has a glassy to waxy luster, smooth, conchoidal fracture surface, and a density and hardness near that of quartz. Porcellanite, on the other hand, has a dull luster, matte to rough surface texture, blocky fracture, and is distinctly less hard and dense than chert.

Steel probes, with hardnesses typically between 5.5 and 6.0, were used to reproducibly discriminate between these two lithologies. When a streak of metal was left on a sample scraped with a medium-light stroke, the rock was termed chert. If the sample was gouged by the probe, it was termed porcellanite.

BIOSTRATIGRAPHY

Time Scale/Chronological Framework

Four microfossil groups were examined for biostratigraphic purposes on Leg 167: diatoms, nannofossils, foraminifers, and radiolarians. Age assignments were primarily made on core-catcher samples. However, additional samples from within the core were studied when a core-catcher sample was found to be inconclusive or otherwise unrepresentative of the core in its entirety.

Because most biostratigraphic datums are not yet calibrated to the Berggren et al. (1995) geomagnetic polarity time scale, zonations were given following the Cande and Kent (1992) time scale. Figure 7 shows correlation of the diatom, nannofossil, foraminifer, and radiolarian zones to the geomagnetic polarity time scale of Cande and Kent (1992).

Neogene planktonic microfossil assemblages in the region of the California Current are intermediate between those of subarctic and subtropical areas. As a result, neither the existing tropical nor the subarctic (high latitude) microfossil zonal schemes were applicable for this region. For the southernmost sites, a few tropical water species were present in sufficient abundance to establish correlation with tropical magnetobiostratigraphic schemes. Likewise, the north subarctic markers were correlated with subarctic magnetobiostratigraphic schemes. Unfortunately, earlier studies of Neogene magnetobiostratigraphy of the California region have relied on incomplete sequences. They provided a foundation for our work, but it appears likely that a magnetobiostratigraphic scheme for the Neogene of California needs to be established during Leg 167.

Biostratigraphy/Paleoenvironments

Diatoms

Zonation

The diatom zonation (Fig. 8) used for the Oligocene and Neogene closely follows the zonation of Barron and Gladenkov (1995) pro-

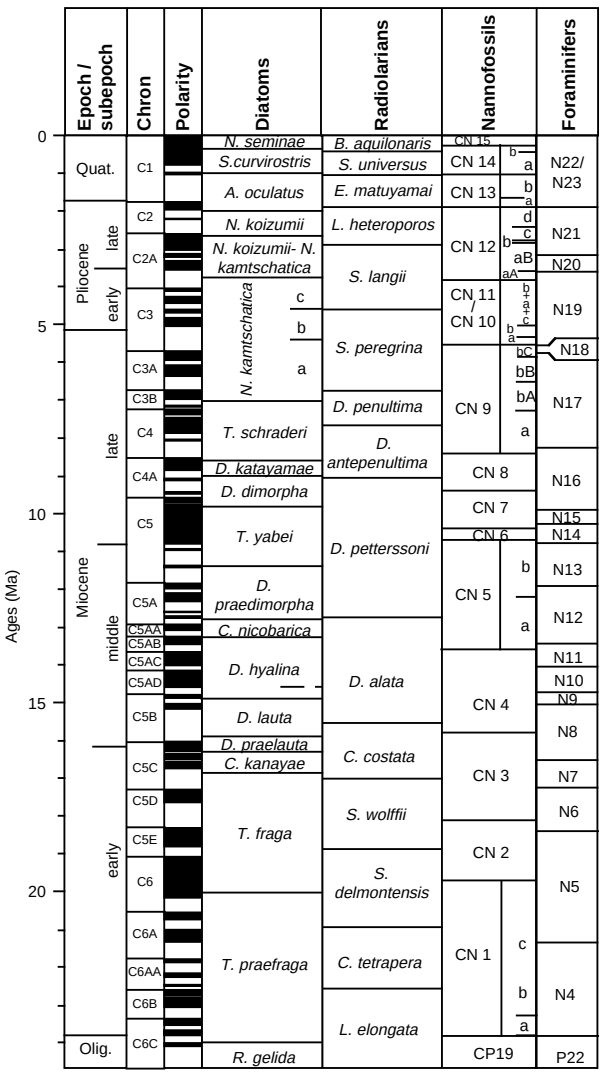

Figure 7. Correlation of the Neogene chronostratigraphy, biostratigraphy, and magnetostratigraphy used during Leg 167. Correlation of the magnetic polarity record and the epoch boundaries follows that of Cande and Kent (1992). Diatom biochronology follows Barron and Gladenkov (1995); foraminifer biochronology follows Blow (1969); nannofossil biochronology follows Okada and Bukry (1980); radiolarian biochronology follows Morley and Nigrini (1995).

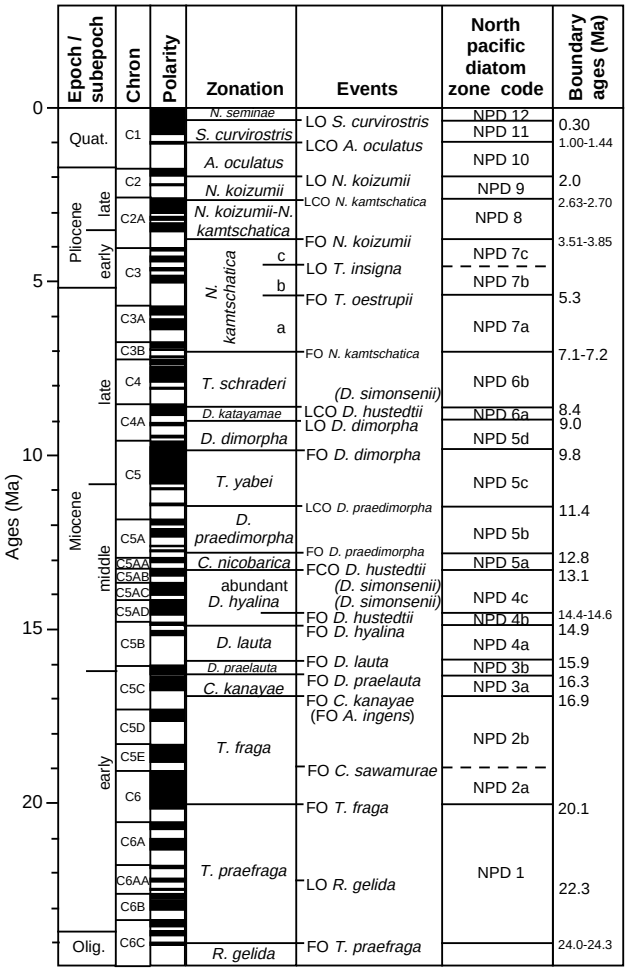

Figure 8. Correlation of diatom zonation, primary zonal markers, and zonal code numbers used on Leg 167. Zone limits have been calibrated to the geochronology of Cande and Kent (1992). LO = last occurrence; LCO = last common occurrence; FO = first occurrence; FCO = first common occurrence.

posed in the Leg 145, North Pacific transect. Code numbers of North Pacific diatom zones by Akiba (1986) were adapted to the above-mentioned zonation with contemporary rearrangement. A slight modification to the zonation used the range of high dominance of *D. hyalina* as a reliable subzone, named the *D. hyalina* abundance Zone (NPD4c), for the uppermost part of the previous *D. hyalina* Zone (old NPD4b), which is within lower middle Miocene sediments. Relationships between the zone name, code label and definition are shown in Table 2.

Datum Levels

Table 3 lists age estimates for the Neogene and Oligocene diatom datum levels that have been found to be useful in the middle-to-high latitudes of the North Pacific. Ages are presented both according to the geomagnetic polarity time scale of Berggren et al. (1985a, 1985b) and of Cande and Kent (1992, 1995).

Methods

Strewn slides were prepared from a small amount of sediment from a core-catcher sample. Another type of strewn slide was produced by placing a sediment sample in a snap-cap vial, adding distilled water, agitating the vial, and removing part of the upper-to-middle suspension with a pipette. When, because of a low concentration of diatom skeletons or an induration of siliceous grains, age assignment control was required, selected samples were processed by boiling them in hydrogen peroxide and hydrochloric acid, followed by centrifuging at 1200 rpm for 2–4 min to remove the chemical solutions from the suspension.

Strewn slides were examined in their entirety at a magnification of 500× for stratigraphic markers and paleoenvironmentally sensitive taxa. Identifications were checked routinely at 1250×. These abundances were recorded as follows:

D (dominant) = more than five specimens per field of view;
A (abundant) = two or more specimens per field of view;
C (common) = one specimen per two fields of view;
F (few) = one specimen per each vertical traverse;
R (rare) = one specimen per a few vertical traverses;
T (trace) = one specimen per several or more vertical traverses; and
B (barren).

Table 2. Diatom zonation and stratigraphic markers used during Leg 167 (modified from Barron and Gladenkov, 1995).

Zone code	Zone	Base	Top
NPD12	*Neodenticula seminae*	LO of *Simonseniella curvirostris*	Present
NPD11	*Simonseniella curvirostris*	LCO of *Actinocyclus oculatus*	LO of *Simonseniella curvirostris*
NPD10	*Actinocyclus oculatus*	LO of *Neodenticula koizumii*	LCO of *Actinocyclus oculatus*
NPD9	*Neodenticula koizumii*	LCO of *N. kamtschatica*	LO of *Neodenticula koizumii*
NPD8	*N. koizumii-N. kamtschatica*	FO of *N. koizumii*	LCO of *N. kamtschatica*
NPD7c	*N. kamtschatica*-c	LO of *Thalassiosira insigna*	FO of *N. koizumii*
NPD7b	*N. kamtschatica*-b	FO of *T. oestrupii*	LO of *Thalassiosira insigna*
NPD7a	*N. kamtschatica*-a	FO of *Neodenticula kamtschatica*	FO of *T. oestrupii*
NPD6b	*Thalassionema schraderi*	LCO of *Denticulopsis hustedtii (simonsenii)*	FO of *Neodenticula kamtschatica*
NPD6a	*Denticulopsis katayamae*	LO of *D. dimorpha*	LCO of *Denticulopsis hustedtii (simonsenii)*
NPD5d	*D. dimorpha*	FO of *D. dimorpha*	LO of *D. dimorpha*
NPD5c	*Thalassiosira yabei*	LCO of *D. praedimorpha*	FO of *D. dimorpha*
NPD5b	*Denticulopsis praedimorpha*	FO of *D. praedimorpha*	LCO of *D. praedimorpha*
NPD5a	*Crucidenticula nicobarica*	FCO of *D. hustedtii (simonsenii)*	FO of *D. praedimorpha*
NPD4c	*Denticulopsis hyalina*-abundance	FO of *D. hustedtii (simonsenii)*	FCO of *D. hustedtii (simonsenii)*
NPD4b	*D. hyalina*	FO of *D. hyalina*	FO of *D. hustedtii (simonsenii)*
NPD4a	*D. lauta*	FO of *D. lauta*	FO of *D. hyalina*
NPD3b	*D. praelauta*	FO of *D. praelauta*	FO of *D. lauta*
NPD3a	*Crucidenticula kanayae*	FO of *Crucidenticula kanayae*	FO of *D. praelauta*
NPD2b	*C. sawamurae*	FO of *C. sawamurae*	FO of *Crucidenticula kanayae*
NPD2a	*Thalassiosira fraga*	FO of *Thalassiosira fraga*	FO of *C. sawamurae*
NPD1	*T. praefraga*	FO of *T. praefraga*	FO of *Thalassiosira fraga*
NPD-gelida	*Rocella gelida*	FO of *Rocella gelida*	FO of *T. praefraga*
NPD-rectus	*Cavitatus rectus*	FO of *Cavitatus rectus*	FO of *Rocella gelida*
NPD-vigilans	*Rocella vigilans*	FO of *Rocella vigilans*	FO of *Cavitatus rectus*

Notes: LO = last occurrence, LCO = last common occurrence, FO = first occurrence, FCO = first common occurrence. Boundaries between NPD4c and NPD5a and between NPD2b and NPD3a can be respectively recognized by the LCO of *Denticulopsis hyalina* and the FO of *Actinocyclus ingens.*

Preservation of diatoms was determined qualitatively as follows:

VG (very good) = finely silicified forms present, no alteration of frustules, and some colonies of frustules preserved;
G (good) = finely silicified forms present and no alteration of frustules observed;
M (moderate) = finely silicified forms present with some alteration; and
P (poor) = finely silicified forms absent or rare and fragmented, and the assemblage is dominated by robust forms.

Foraminifers

Chronological Framework

Direct application of middle- and low-latitude zonations such as that of Blow (1969) are often difficult or inappropriate for California Margin Neogene sequences because of the cool to temperate nature of the faunas. Foraminiferal age determinations for Leg 167 were based on the datum levels of Blow (1969) whenever possible, with modifications of the Neogene zonations by Kennett and Srinivasan (1983). For the higher temperate latitudes of the North Pacific (Fig. 9), ages were also constrained by the chronostratigraphic frameworks developed by Lagoe and Thompson (1988) and, for lower temperate latitudes, by Barron and Keller (1983). This framework was based on planktonic foraminiferal evolutionary datums (first and last occurrences) and paleoclimatically controlled coiling shifts in *Neogloboquadrina pachyderma* (Table 4) from over twenty locations in the North Pacific Ocean (see Lagoe and Thompson, 1988). Lagoe and Thompson (1988) constructed a generalized coiling curve for the northeastern Pacific containing 16 correlative coiling intervals (CD = Coiling Dominance; Fig. 9). For shipboard purposes the "CD1–7" intervals of Lagoe and Thompson (1988) were grouped as "CD1–7" representing a zone of high-frequency coiling shifts with mixed coiling directions from 367 ka to the present. Age determinations based on foraminifers are improved by integrating the coiling shifts with the zonation of Blow (1969).

Methods

Sediment samples of approximately 30 cm^3 were taken from each core catcher. They were disaggregated in a Calgon solution and then washed with tap water over a 63-µm sieve. Samples that were difficult to disaggregate were pretreated with a 3% hydrogen peroxide solution. Sieves were soaked in a solution of methylene blue carbonate stain between samples to identify potential contamination. Residues were filtered and dried in an oven or under a heat lamp. Age assignments were primarily made from core-catcher samples.

Three classes of foraminiferal preservation were used:

G (good) = >90% of the specimens were unbroken and well preserved;
M (moderate) = 30%–90% of the specimens were fragmented or showed evidence of dissolution/or recrystallization; and
P (poor) = almost all specimens were fragmented and showed evidence of dissolution and/or recrystallization.

Planktonic Foraminifers

Planktonic foraminiferal abundance was defined as follows:

R (rare) = <10 specimens/20 cm^3;
F (few) = 10–100 specimens/20 cm^3;
C (common) = (101–500 specimens/20 cm^3;
A (abundant) = >500 specimens/20 cm^3; and
B (barren).

Paleoenvironmental Analysis

Benthic foraminifers were examined in the >150-µm size fraction primarily for paleoenvironmental analysis and interpretation of paleobathymetry. Benthic faunal assemblages from the continental margins of North America are strongly affected by large changes in the concentrations of oxygen of bottom waters and surface sediments. Low oxygen concentrations are widespread in the basins of the Southern California Borderland province and are also associated with the oxygen minimum zone of the continental margin. We made general evaluations of the oxygen concentrations (low, moderate, or high) of samples as indicated by the benthic foraminiferal assemblages, similar to those carried out by Kennett, Baldauf, and Lyle (1995) for Santa Barbara Basin late Quaternary assemblages. Paleobathymetric zonation was based on Ingle (1980) as follows: neritic (0–150 m); upper bathyal (150–500 m); middle bathyal (500–2000 m); lower bathyal (2000–4000 m); and abyssal (4000–6000 m).

Table 3. Magnetic calibration and estimated ages of diatom events used during Leg 167, based on the time scales of Berggren et al. (1985a, 1985b) and Cande and Kent (1992, 1995).

Event	Datum	Berggren (Ma)	CK92 (Ma)	CK95 (Ma)	Chron	Source
LO	*Simonseniella curvirostris*	0.3–0.35	0.30	0.30	C1n.1n	3
LO	*Thalassiosira jouseae*	0.28–0.39	0.30–0.41	0.30–0.41	C1n.1n	1
LO	*Rhizosolenia matuyamai*	0.85–0.97	0.91–1.04	0.91–1.06	C1n.2n	1
FO	*Rhizosolenia matuyamai*	0.91–1.05	0.98–1.12	0.99–1.14	C1n.2n	1
LCO	*Actinocyclus oculatus*	0.93–1.33	1.00–1.44	1.01–1.46	C1n.2n	1
FO	*Simonseniella curvirostris*	1.5	1.58		C1r.2r	1
LO	*Coscinodiscus pustulatus*	1.7	1.8			4
LO	*Pyxidicula horridus*	1.7	1.8–2.0	1.8–2.0		2
LO	*Thalassiosira antiqua*	1.43–1.7	1.5–1.8	1.52–1.8		1
LO	*Neodenticula koizumii*	1.9	2.0	2.0	C2r.1r	3
LO	*Pyxidicula pustulata*	2.0	2.0–2.2	2.0–2.14		4
LO	*Thalassiosira convexa*	2.3	2.4	2.35	C2r.1r	2
LCO	*Neodenticula kamtschatica*	2.5–2.58	2.63–2.7	2.61–2.68	C2An.1n	1
FO	*Neodenticula seminae*	2.6	2.7	2.68	C2An.1n	3
LO	*Thalassiosira marujamica*		3.1–3.2	3.08–3.2	C2An.1r to .2n	8
LO	*Thalassiosira jacksonii*	3.1	3.1–3.4	3.08–3.41	C2An.1r to .3n	3
FO	*Neodenticula koizumii*	3.6	3.51–3.85	3.53–3.95	C2A.3r	1
FO	*Actinocyclus oculatus*	3.7	3.6–3.9	3.64–4.01	C2A.3r	3
FO	*Thalassiosira latimarginata*	4.9	4.9	5.07	C3n.4n	8
FO	*Thalassiosira oestrupii*	5.1	5.3	5.49	C3n.4n	2
LO	*Rouxia californica*	5.2	5.5			2
LO	*Thalassiosira miocenica*	5.35	5.8	6.0	C3An.1n	1
FO	*Thalassiosira praeoestrupii*	5.54	5.95	6.1	C3An.1r	8
LO	*Thalassiosira praeconvexa*	5.8	6.3		C3An.2n	2
FO	*Thalassiosira miocenica*	6.1	6.2	6.4	C3Ar.2n	2
LO	*Cavitatus jouseanus*		6.5–6.6	6.7–6.8	C3Ar.2r	8
FO	*Thalassiosira jacksonii*	6.4	6.8			2
FO	*Nitzschia reinholdii*	6.5	7.2–7.3	7.4–7.5	C4n.1n	8
FO	*Neodenticula kamtschatica*	6.6	7.1–7.2	7.3–7.4	C3Br	8
LO	*Thalassionema schraderi*	6.7	7.4	7.6	C4n.1r	8
LO	*Thalassiosira minutissima*	7.5	8.2			2
FO	*Thalassiosira antiqua*	7.6	8.3	8.5		2
LO	*Denticulopsis katayamae*	7.6	8.3	8.5		2
FO	*Thalassiosira marujamica*	7.9–7.8	8.4–8.5			2
LCO	*Denticulopsis hustedtii*	8	8.4	8.6	C4n.1r	8
FO	*Thalassionema schraderi*	8	8.6			2
LO	*Lithodesmium reynoldsii*	8.1	8.7			2
LO	*Denticulopsis dimorpha*	8.4	9	9.16	C4n.1r	8
FO	*Denticulosis katayamae*	8.7	9.1	9.26	C4Ar.1n	8
FO	*Thalassionema schraderi*		9.3	9.5	C4Ar.1r	8
FO	*Thalassiosira minutissima*	9	9.6			2
FO	*Denticulopsis dimorpha*	8.9	9.8	9.9	C5n.2n	8
LO	*Nitzschia heteropolica*		10.7–10.9	10.8–11.0	ca.C5n.2n base	8
LO	*Medialia splendida*		10.7–10.9	10.8–11.0	ca.C5n.2n base	8
LCO	*Denticulopsis praedimorpha*	10.4	11.4	11.5	C5r.2n	8
FO	*Hemidiscus cuneiformis*	11.4	11.7			2
FO	*Thalassiosira brunii*	11.5	11.8			2
FO	*Simonseniella barboi*	11.2	12.2	12.3	C5An.2n	8
LO	*Crucidenticula nicobarica*	12.2	12.4	12.5		2
FO	*Denticulopsis praedimorpha*	12.6	12.8	12.9	C5Ar.2r	5
FCO	*Denticulopsis hustedtii*	13.65	13.1	13.1	C5AAr	2
LO	*Thalassiosira praeyabei*	13.4	13.4			2
FO	*Thalassiosira grunowii*	13.75	13.7			2
FO	*Dentiuclopsis hustedtii*	14.3	14.4–14.6	14.4–14.6	C5AnDn	8
FO	*Thalassiosira praeyabei*	14.8	14.7			2
LO	*Crucidenticula kanayae*	14.8	14.7			2
FO	*Denticulopsis hyalina*	15	14.9	14.9	C5Bn.1r	8
FO	*Actinocyclus ingens nodus*	15.2	15.1	15.1		2
LO	*Denticulopsis praelauta*	15.3–15.7	15.2–15.6			2
FO	*Denticulopsis lauta*	16	15.9	15.9		2
FO	*Denticulopsis praelauta*	16.3	16.3	16.3		2
FO	*Crucidenticula kanayae*	18	16.9	16.9	C5Cn.3r	8
FO	*Actinocyclus ingens*	17.9	17.6			2
LO	*Crucidenticula sawamurae*	17.8	18.4	18.4	C5En	2
FO	*Thalassiosira fraga*	20.3–20.4	20.1	20.1	C6An.2n	7
LO	*Rocella gelida*	21.8–22.1	22.3	22.3	C6AAr.1r	7
FO	*Thalassiosira spumellaroides*	22.6	22.6			6
FO	*Thalassiosira praefraga*		24.0–24.3	24.0–24.3		7
FO	*Thalassiosira spinosa*	24.0–24.5	24.0–24.3			7
LO	*Lisitzinia ornata*	24.5	24.3	24.3	C6Cr.3r	6
LO	*Rocella vigilans*	26.3	25.4		C7r	6
FO	*Rocella gelida*	27.4–27.6	26.2–26.4	26.2–26.4	C8n.2n	7
FO	*Lisitzinia ornata*	29.2	27.9	27.9	C9r.2r	6
FO	*Rocella vigilans*	32.2	30.2	30.2	C11r.2r	6
LO	*Pyxilla reticulata*	32.3	30.3	30.3	C11r.2r	6
FO	*Cavitatus jouseana*	32.6	30.6	30.6	C12n.1n	6
LO	*Rhizosolenia oligocaenica*	33.3–33.4	31.0–31.1	31.0–31.1	C12r.1r	6
FO	*Rhizosolenia oligocaenica*	35.9–36.0	33.6–33.7	33.6–33.7	C13r.2r	7

Notes: Same abbreviations as in Table 2. Sources: 1 = Koizumi and Tanimura (1985); 2 = Barron (1992); 3 = Koizumi (1992); 4 = Barron (1980); 5 = Gersonde and Burckle (1990); 6 = Harwood and Maruyama (1992); 7 = Baldauf and Barron (1991); 8 = Barron and Gladenkov (1995).

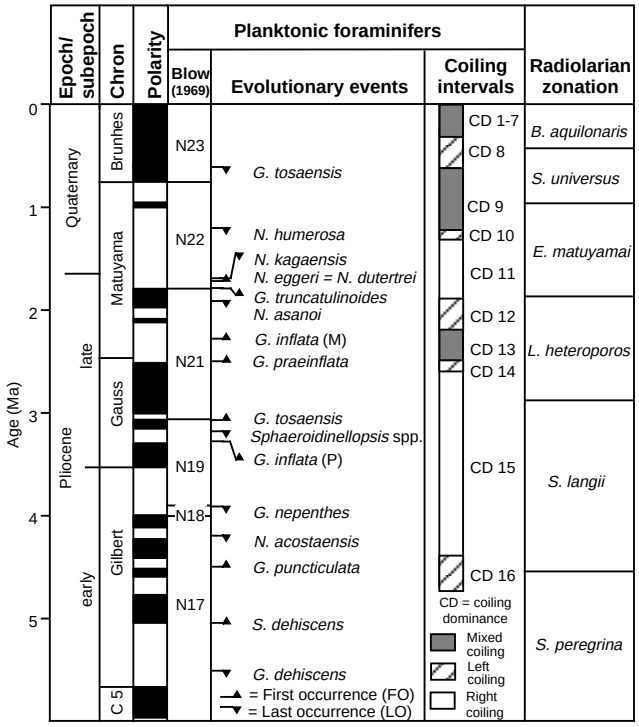

Figure 9. Correlation of radiolarian zones, planktonic foraminiferal zonation of Blow (1969), planktonic foraminiferal evolutionary events, and coiling zones of *Neogloboquadrina pachyderma* used on Leg 167 (see text) to the geomagnetic polarity time scale of Cande and Kent (1992).

Table 4. Ages of events in chronostratigraphic framework of Lagoe and Thompson (1988), converted to the time scale of Cande and Kent (1992).

	Event	Age* (Ma)	Age** (Ma)
	CD1–7/CD8 boundary	0.37	0.37
	CD8/CD9 boundary	0.6	0.6
F1	LO *Globorotalia tosaensis*	0.6	0.6
F2	LO *Neogloboquadrina humerosa*	1.1	1.2
	CD9/CD10 boundary	1.15	1.23
	CD10/CD11 boundary	1.3	1.4
F3	LO *Neogloboquadrina kagaensis*	1.6	1.7
F4	FO *Neogloboquadrina eggeri = N. dutertrei*	1.66	1.76
F5	FO *Globorotalia truncatulinoides*	1.7	1.8
	CD11/CD12 boundary	1.8	1.9
F6	LO *Neogloboquadrina asanoi*	1.85	1.9
	CD12/CD13 boundary	2.1	2.2
F7	FO *Globorotalia inflata* (modern form)	2.2	2.4
	CD13/CD14 boundary	2.4	2.5
	CD14/CD15 boundary	2.5	2.6
F8	FO *Globorotalia praeinflata*	2.5	2.6
F9	FO *Globorotalia tosaensis*	3.0	3.1
F10	LO *Sphaeroidinellopsis* spp.	3.1	3.2
F11	FO *Globorotalia inflata* (primitive form)	3.2	3.3
F12	LO *Globigerina nepenthes*	3.7	3.9
F13	LO *Neogloboquadrina acostaensis*	4.0	4.2
	CD15/CD16 boundary	4.2	4.4
F14	FO *Globorotalia puncticulata*	4.4	4.6
F15	FO *Sphaeroidinella dehiscens*	5.2	5.3

Notes: CD = coiling dominance. Coiling intervals: even (left coiling); odd (right coiling); CD1–7 (high-frequency mixed coiling interval). Abbreviations used: FO = first occurrence; LO = last occurrence. * = age estimates found by using time scale of Berggren et al. (1985a, 1985b); ** = age estimates found by using time scale of Cande and Kent (1992).

Calcareous Nannofossils

During Leg 167 we used the zonal scheme of Okada and Bukry (1980). This scheme is presented in Figure 7. The Cenozoic biostratigraphic events used are listed in Table 5. Events have been tied directly to magnetostratigraphic records, many of which are derived from extra-tropical region. Note that almost all the events of Okada and Bukry (1980) are listed in Table 5. If they are not accounted, it is because we considered them inadequately correlated to the magnetostratigraphic record. Questionable placement of the base of CN14a and the base of CN13b arose from taxonomic ambiguities.

Methods

Calcareous nannofossils were examined by means of standard light microscope techniques, under crossed nicols and transmitted light at 1000× magnification.

The nannofossil assemblages at times showed signs of strong etching and/or strong overgrowth: more dissolution-resistant forms apparently accrete calcite derived from dissolution of other forms. To characterize these states of preservation we have adopted a code described already for ODP Leg 154 as follows:

G (good) = little or no evidence of dissolution and/or secondary overgrowth of calcite; diagnostic characters fully preserved;
M (moderate) = dissolution and/or secondary overgrowth; partially altered primary morphological characteristics; however, nearly all specimens can be identified at the species level; and
P (poor) = severe dissolution, fragmentation, and/or secondary overgrowth with primary features largely destroyed: many species cannot be identified at the species level and/or generic level.

We have used the following levels of relative abundance for nannofossil assemblages:

D (dominant) = the taxonomic category constitutes >50% of the total assemblage;
A (abundant) = the taxonomic category constitutes from 10% to 50% of the total assemblage;
C (common) = the taxonomic category constitutes from 1% to 10% of the total assemblage;
F (few) = the taxonomic category constitutes from 0.1% to 1% of the total assemblage;
R (rare) = the taxonomic category constitutes <0.1% of the total assemblage;
RR (very rare) = one specimen every three vertical traverses;
P (present) = one specimen per 10 fields of view; and
B (barren).

Radiolarians

Zonation

Because of the location of the Leg 167 sites at the boundary between the tropical Pacific and the California Current area, two zonations were chosen. The eastern tropical Pacific zonation (Table 6) follows the classical tropical zonation (Sanfilippo et al., 1985), completed by Johnson et al. (1989), and emended by Moore (1995). The temperate zonation (Table 6) follows the middle-to-North-Pacific zonation published by Morley and Nigrini (1995). Table 7 lists radiolarian species events from both the temperate and eastern tropical Pacific.

Table 5. Magnetic calibration and the estimated ages of Neogene calcareous nannofossil events used during Leg 167, based on the time scale of Shackleton et al. (1995).

Event	Zone (base)	Age (Ma)	Sources
B acme *Emiliania huxleyi*		0.085	1
B *Emiliania huxleyi*	CN15	0.26	1
T *Pseudoemiliania lacunosa*	CN14b	0.46	1
Re-entrance medium *Gephyrocapsa* spp.	CN14a?	1.02	2
T large *Gephyrocapsa* spp.		1.24	2
B large *Gephyrocapsa* spp.		1.44	2
T *Helicosphaera sellii*		1.47	2
T *Calcidiscus macintyrei*		1.58	2
B medium *Gephyrocapsa* spp.	CN13b?	1.69	2
T *Discoaster brouweri*	CN13a	1.96	2
B acme *Discoaster triradiatus*		2.15	2
T *Discoaster pentaradiatus*	CN12d	2.52	3
T *Discoaster surculus*	CN12c	2.63	3
T *Discoaster tamalis*	CN12b	2.78	3
T *Sphenolithus* spp.	CN12aB	3.66	3
T *Reticulofenestra pseudoumbilicus*	CN12aA	3.82	3
B *Ceratolithus acutus*	CN10b	4.99	4
B *Ceratolithus rugosus*	CN10c	5.07	3
T *Triquetrorhabdulus rugosus*		5.35	4
T *Discoaster quinqueramus*	CN10a	5.55	4
T *Amaurolithus amplificus*	CN9bC	5.93	4
B *Amaurolithus amplificus*	CN9bB	6.5	4
T paracme *R. pseudoumbilicus*		6.76	4
B *Amaurolithus primus*	CN9bA	7.17	4
Bc *Discoaster surculus*		7.8	4
B *Discoaster berggrenii*	CN9a	8.4	4
B paracme *R. pseudoumbilicus*		8.71	4
T *Catinaster calyculus*		9.4	*
T *Discoaster hamatus*	CN8a	9.4	4
B *Minylitha convallis*		9.37	4
B *Discoaster neohamatus*		9.6	4
B *Discoaster hamatus*	CN7	10.38	4
B *Catinaster coalitus*	CN6	10.7	4
T *Coccolithus miopelagicus*		10.48	*
Tc *Discoaster kugleri*		11.35	4
Bc *Discoaster kugleri*		11.7	4
T *Coronocyclus nitescens*		12.12	4
B *Discoaster kugleri*	CN5b	12.2	4
B *Calcidiscus macintyrei* ≥11 µm		12.3	4
B *Triquetrorhabdulus rugosus*		12.62	4
T *Calcidiscus premacintyrei*		12.14	4
T *Discoaster signus*		13.08	4
Tc *Cyclicargolithus floridanus*		13.19	4
T *Sphenolithus heteromorphus*	CN5a	13.6	4
T *Helicosphaera ampliaperta*	CN4	15.8	5
B *Discoaster signus*		16.22	4
T abundant *Discoaster deflandrei*		16.22	4
B *Calcidiscus premacintyrei*		17.4	6
B *Sphenolithus heteromorphus*	CN3	18.1	7
T *Sphenolithus belemnos*		18.4	7
B *Sphenolithus belemnos*	CN2	19.7	7
T *Triquetrorhabdulus carinatus*		23.1	7
B *Discoaster druggi*	CN1c	23.3	8
T acme *Sphenolithus delphix*		23.7	9
T *Dictyococcites bisectus*	CN1c	23.8	10
B acme *Sphenolithus delphix*		24.4	9
T *Sphenolithus ciperoensis*	CN1a	24.7	11

Notes: B = base; T = top; Bc = base continuous; Tc = top continuous. Sources: 1 = Thierstein et al. (1977); 2 = Raffi et al. (1993); 3 = Backman and Shackleton (1983); 4 = Raffi and Flores (1995); 5 = Backman et al. (1990); 6 = Gartner (1992); 7 = Olafsson (1991); 8 = Berggren et al. (1985a); 9 = Fornaciari et al. (1990); 10 = Berggren et al. (1985b); 11 = Olafsson and Villa (1992); * = Site 925, Leg 154.

Methods

Sample preparation for microscopic examination during Leg 167 followed the standard techniques described by Sanfilippo et al. (1985). All samples were treated with acid and sieved at 63 µm, with the coarse fraction retained for slide preparation. When the acid-treated residues contained large clumps of clay aggregates, the coarse fraction was further treated with a strong base (NaOH) for several minutes, then briefly immersed in an ultrasonic bath and resieved.

For each sample examined, qualitative estimates of radiolarian abundance and preservation were made. Radiolarian assemblage abundance was assessed as follows:

A (abundant) = >500 specimens on slide;
C (common) = 100–500 specimens on slide;
F (few) = 50–100 specimens on slide;
R (rare) = <50 specimens on slide;
T (trace) = one specimen found; and
B (barren).

Preservation of the radiolarian assemblage was based on the following:

G (good) = radiolarians show no sign of dissolution with only minor fragmentation;
M (moderate) = radiolarians show evidence of moderate dissolution with obvious fragmentation; and
P (poor) = radiolarians show signs of a high degree of dissolution with very few intact specimens.

PALEOMAGNETISM

Laboratory Facilities and Procedures

The remanent magnetization of archive-half sections was measured on a 2G Enterprises 760R magnetometer using a standard 10-cm reading interval before and after alternating field (AF) demagnetization. The demagnetization treatment applied to these sections, usually one AF demagnetization step, was selected based on the results of progressive AF demagnetization experiments conducted on pilot sections from the archive half and discrete samples from the working half. The peak field during AF demagnetization of the archive half was mainly 20 mT and, in a few cases, 25 mT. Test measurements of weak sections showed that the magnetometer can measure magnetizations reliably above 1 mA/m. The direction of magnetization could not be determined well for intensities below 1 mA/m.

The magnetic susceptibility was measured for each whole-core section as part of the multisensor track (MST) analyses. Discrete sample remanence measurements were made with a Minispin magnetometer. As a magnetic polarity time scale for Leg 167, we chose Cande and Kent's (1995) seafloor spreading–based time scale, in agreement with the biostratigraphers and stratigraphic correlators.

Core Orientation and Sampling

All paleomagnetic measurements made during Leg 167 for the split-core sections and discrete samples follow the standard ODP core orientation scheme. During APC drilling, core orientation was achieved with a Tensor orientation tool in one hole per site. Data from the Tensor tool were corrected for local magnetic variation before their use in the computation of remanence field directions. Oriented discrete samples were taken from the working-half cores by pressing a 6-cm^3 sample cube into soft sediment. To minimize sediment deformation, a thin ceramic knife was used to cut into more lithified sediment before inserting the sample cubes.

COMPOSITE DEPTHS

Composite Section Development

The recovery of continuous sections over APC-cored intervals of the sedimentary sequence was crucial to the paleoceanographic objectives of Leg 167. Drilling multiple APC holes at each site that are offset in depth helped to ensure that intervals of no recovery in a single APC hole were recovered in an adjacent hole. During Leg 167, as with previous ODP legs, the continuity of recovery was confirmed by developing composite depth sections at the multiple-cored sites. The methods used for composite section development during Leg 167 are

Table 6. Radiolarian zonations and stratigraphic markers used in Leg 167.

	Definition of base	Age (Ma, CK92) and source	Definition of top	Age (Ma, CK92) and source	Author
Tropical Pacific zonation					
Buccinosphaera invaginata	FO *Buccinosphaera invaginata*	0.18 (Johnson et al., 1989)	Holocene		Nigrini, 1971
Collosphaera tuberosa	LO *Stylatractus universus*	0.46 (Moore, 1995)	FO *Buccinosphaera invaginata*	0.18 (Johnson et al., 1989)	Nigrini, 1971
Stylatractus universus	FO *Collosphaera tuberosa*	0.61 (Moore, 1995)	LO *Stylatractus universus*	0.46 (Shackleton et al., 1995)	Johnson et al., 1989; Moore, 1995
Amphirhopalum ypsilon	LO *Anthocyrtidium angulare*	1.08 (Caulet et al., 1993)	FO *Collosphaera tuberosa*	0.61 (Shackleton et al., 1995)	Nigrini, 1971
Anthocyrtidium angulare	LO *Pterocanium prismatium*	1.73 (Moore, 1995)	LO *Anthocyrtidium angulare*	1.08 (Caulet et al., 1993)	Nigrini, 1971
Pterocanium prismatium	LO *Stichocorys peregrina*	2.55 (Moore, 1995)	LO *Pterocanium prismatium*	1.73 (Moore, 1995)	Riedel & Sanfilippo, 1970; amend. Moore, 1995
Anthocyrtidium jenghisi	LO *Phormostichoartus doliolum*	3.43 (Moore, 1995)	LO *Stichocorys peregrina*	2.55 (Moore, 1995)	Johnson et al., 1989; amend. Moore, 1995
Phormostichoartus doliolum	LO *Didymocyrtis penultima*	4.04 (Moore, 1995)	LO *Phormostichoartus doliolum*	3.43 (Moore, 1995)	Johnson et al., 1989; amend. Moore, 1995
Stichocorys peregrina	*Stichocorys delmontensis –> Stichocorys peregrina*	6.42 (Moore, 1995)	LO *Didymocyrtis penultima*	4.04 (Moore, 1995)	Riedel & Sanfilippo, 1970, amend. 1978; amend. Moore, 1995
Didymocyrtis penultima	LO *Diartus hughesi*	7.67 (Moore, 1995)	*Stichocorys delmontensis –> Stichocorys peregrina*	6.42 (Moore, 1995)	Riedel & Sanfilippo, 1970, amend. 1978
Didymocyrtis antepenultima	*Diartus petterssoni –> Diartus hughesi*	8.55 (Moore, 1995)	LO *Diartus hughesi*	7.67 (Moore, 1995)	Riedel & Sanfilippo, 1970, amend. 1978
Diartus petterssoni	FO *Diartus petterssoni*	11.86 (Moore, 1995)	*Diartus petterssoni –> Diartus hughesi*	8.55 (Moore, 1995)	Riedel & Sanfilippo, 1970, amend. 1978
Dorcadospyris alata	*Dorcadospyris dentata –> Dorcadospyris alata*	15.69 (Moore, 1995)	FO *Diartus petterssoni*	11.86 (Moore, 1995)	Riedel & Sanfilippo, 1970, amend. 1978
Calocycletta costata	FO *Calocycletta costata*	17.05 (Lazarus et al., 1995)	*Dorcadospyris dentata –> Dorcadospyris alata*	15.69 (Moore, 1995)	Riedel & Sanfilippo, 1970
Stichocorys wolffii	FO *Stichocorys wolffii*	17.95 (Lazarus et al., 1995)	FO *Calocycletta costata*	17.05 (Lazarus et al., 1995)	Riedel & Sanfilippo, 1978
Stichocorys delmontensis	LO *Theocyrtis annosa*	20.56 (Lazarus et al., 1995)	FO *Stichocorys wolffii*	17.95 (Lazarus et al., 1995)	Riedel & Sanfilippo, 1978
Cyrtocapsella tetrapera	FO *Cyrtocapsella tetrapera*	23.69 (Sanfilippo & Nigrini, 1995)	LO *Theocyrtis annosa*	20.56 (Lazarus et al., 1995)	Riedel & Sanfilippo, 1978
Lychnocanoma elongata	FO *Lychnocanoma elongata*	24.60 (Sanfilippo & Nigrini, 1995)	FO *Cyrtocapsella tetrapera*	23.69 (Sanfilippo & Nigrini, 1995)	Riedel & Sanfilippo, 1970, amend. 1978
Buccinosphaera invaginata	FO *Buccinosphaera invaginata*	0.18 (Johnson et al., 1989)	Holocene		Nigrini, 1971
Collosphaera tuberosa	LO *Stylatractus universus*	0.46 (Moore, 1995)	FO *Buccinosphaera invaginata*	0.18 (Johnson et al., 1989)	Nigrini, 1971
Stylatractus universus	FO *Collosphaera tuberosa*	0.61 (Moore, 1995)	LO *Stylatractus universus*	0.46 (Shackleton et al., 1995)	Johnson et al., 1989; Moore, 1995
Amphirhopalum ypsilon	LO *Anthocyrtidium angulare*	1.08 (Caulet et al., 1993)	FO *Collosphaera tuberosa*	0.61 (Shackleton et al., 1995)	Nigrini, 1971
Anthocyrtidium angulare	LO *Pterocanium prismatium*	1.73 (Moore, 1995)	LO *Anthocyrtidium angulare*	1.08 (Caulet et al., 1993)	Nigrini, 1971
Pterocanium prismatium	LO *Stichocorys peregrina*	2.55 (Moore, 1995)	LO *Pterocanium prismatium*	1.73 (Moore, 1995)	Riedel & Sanfilippo, 1970; amend. Moore, 1995
Anthocyrtidium jenghisi	LO *Phormostichoartus doliolum*	3.43 (Moore, 1995)	LO *Stichocorys peregrina*	2.55 (Moore, 1995)	Johnson et al., 1989; amend. Moore, 1995
Phormostichoartus doliolum	LO *Didymocyrtis penultima*	4.04 (Moore, 1995)	LO *Phormostichoartus doliolum*	3.43 (Moore, 1995)	Johnson et al., 1989; amend. Moore, 1995
Stichocorys peregrina	*Stichocorys delmontensis –> Stichocorys peregrina*	6.42 (Moore, 1995)	LO *Didymocyrtis penultima*	4.04 (Moore, 1995)	Riedel & Sanfilippo, 1970, amend. 1978; amend. Moore, 1995
Didymocyrtis penultima	LO *Diartus hughesi*	7.67 (Moore, 1995)	*Stichocorys delmontensis –> Stichocorys peregrina*	6.42 (Moore, 1995)	Riedel & Sanfilippo, 1970, amend. 1978
Didymocyrtis antepenultima	*Diartus petterssoni –> Diartus hughesi*	8.55 (Moore, 1995)	LO *Diartus hughesi*	7.67 (Moore, 1995)	Riedel & Sanfilippo, 1970, amend. 1978
Diartus petterssoni	FO *Diartus petterssoni*	11.86 (Moore, 1995)	*Diartus petterssoni –> Diartus hughesi*	8.55 (Moore, 1995)	Riedel & Sanfilippo, 1970, amend. 1978
Dorcadospyris alata	*Dorcadospyris dentata –> Dorcadospyris alata*	15.69 (Moore, 1995)	FO *Diartus petterssoni*	11.86 (Moore, 1995)	Riedel & Sanfilippo, 1970, amend. 1978
Calocycletta costata	FO *Calocycletta costata*	17.05 (Lazarus et al., 1995)	*Dorcadospyris dentata –> Dorcadospyris alata*	15.69 (Moore, 1995)	Riedel & Sanfilippo, 1970
Stichocorys wolffii	FO *Stichocorys wolffii*	17.95 (Lazarus et al., 1995)	FO *Calocycletta costata*	17.05 (Lazarus et al., 1995)	Riedel & Sanfilippo, 1978
Stichocorys delmontensis	LO *Theocyrtis annosa*	20.56 (Lazarus et al., 1995)	FO *Stichocorys wolffii*	17.95 (Lazarus et al., 1995)	Riedel & Sanfilippo, 1978
Cyrtocapsella tetrapera	FO *Cyrtocapsella tetrapera*	23.69 (Sanfilippo & Nigrini, 1995)	LO *Theocyrtis annosa*	20.56 (Lazarus et al., 1995)	Riedel & Sanfilippo, 1978
Lychnocanoma elongata	FO *Lychnocanoma elongata*	24.60 (Sanfilippo & Nigrini, 1995)	FO *Cyrtocapsella tetrapera*	23.69 (Sanfilippo & Nigrini, 1995)	Riedel & Sanfilippo, 1970, amend. 1978
North Pacific zonation					
Botryostrobus aquilonaris	LO *Stylatractus universus*	0.55 (Morley & Nigrini, 1995)	Holocene		Hays, 1970
Stylatractus universus	LO *Eucyrtidium matuyamai*	1.0 (Morley & Nigrini, 1995)	LO *Stylatractus universus*	0.55 (Morley & Nigrini, 1995)	Hays, 1970
Eucyrtidium matuyamai	*Eucyrtidium calvertense –> Eucyrtidium matuyamai*	2.0 (Morley & Nigrini, 1995)	LO *Eucyrtidium matuyamai*	1.0 (Morley & Nigrini, 1995)	Hays, 1970
Sphaeropyle langii	FO *Sphaeropyle langii*	5.0-6.0 (~45° N), 4.8 (~51° N) (Morley & Nigrini, 1995)	*Eucyrtidium calvertense –> Eucyrtidium matuyamai*	2.0 (Morley & Nigrini, 1995)	Foreman, 1975
Stichocorys peregrina	*Stichocorys delmontensis –> Stichocorys peregrina*	7.55 (Morley & Nigrini, 1995)	FO *Sphaeropyle langii*	5.0-6.0 (~45° N), 4.8 (~51° N) (Morley & Nigrini, 1995)	Riedel and Sanfilippo, 1970
Didymocyrtis penultima	LO *Diartus hughesi*	7.7 (Spencer-Cervato et al., 1993)	*Stichocorys delmontensis –> Stichocorys peregrina*	7.55 (Morley & Nigrini, 1995)	Riedel and Sanfilippo, 1970, amend. 1978
Didymocyrtis antepenultima	*Diartus petterssoni –> Diartus hughesi*	11.53 (Spencer-Cervato et al., 1993)	LO *Diartus hughesi*	7.7 (Spencer-Cervato et al., 1993)	Riedel and Sanfilippo, 1970, amend. 1978
Diartus petterssoni	FO *Diartus petterssoni*	12.14 (Spencer-Cervato et al., 1993)	*Diartus petterssoni –> Diartus hughesi*	11.53 (Spencer-Cervato et al., 1993)	Riedel and Sanfilippo, 1970, amend. 1978
Dorcadospyris alata	*Dorcadospyris dentata –> Dorcadospyris alata*		FO *Diartus petterssoni*	12.14 (Spencer-Cervato et al., 1993)	Riedel and Sanfilippo, 1970, amend. 1971

Notes: Tropical zonation after Riedel and Sanfilippo (1970, 1978), completed by Johnson et al. (1989), and emended by Moore (1995). Zonal marker calibration follows the time scale of Shackleton et al. (1995) for the time interval between the Holocene and 16 Ma, and the 1992 time scale of Cande and Kent (CK92) for the older interval. North Pacific zonation after Morley and Nigrini (1995); calibration of zonal markers follows the time scale of Cande and Kent (1992).

Table 7. Estimated ages of Neogene tropical and temperate radiolarian events used during Leg 167.

Event	Species	Age (Ma)	Source
LO	*Lychnocanoma sakai*	0.05	1
LO	*Stylacontarium acquilonium*	0.4	1
LO	*Stylatractus universus**	0.41	2
LO	*Stylatractus universus***	0.55	1
FO	*Collosphaera tuberosa*	0.61	2
LO	*Anthocyrtella? callopisma*	0.65	1
FO	*Lamprocyrtis nigriniae***	0.8–1.2	1
LO	*Lamprocyrtis neoheteroporos*	0.9	1
LO	*Eucyrtidium matuyamai*	1.0	1
LO	*Theocorythium vetulum*	1.22	2
FO	*Lamprocyrtis nigriniae**	1.23	2
FO	*Pterocorys minythorax*	1.55	2
LO	*Lamprocyrtis heteroporos**	1.61	2
LO	*Lamprocyrtis heteroporos***	1.7	1
LO	*Sphaeropyle robusta*	1.5/1.7	1
LO	*Pterocanium prismatium*	1.74	2
FO	*Anthocyrtidium angulare*	1.77	2
FO	*Eucyrtidium matuyamai*	2.0	1
LO	*Anthocyrtidium jenghisi*	2.4	2
FO	*Lamprocyrtis neoheteroporos***	2.6/2.8	1
FO	*Cycladophora d. davisiana**	2.71	2
LO	*Stichocorys peregrina**	2.76	2
FO	*Cycladophora d. davisiana***	2.9	1
FO	*Lamprocyrtis neoheteroporos**	3.06	2
FO	*Lamprocyrtis heteroporos**	3.06	2
FO	*Anthocyrtidium pliocenica*	3.36	2
LO	*Phormostichoartus fistula*	3.67	2
LO	*Lychnodictyum audax*	3.78	2
LO	*Phormostichoartus doliolum*	3.89	2
FO	*Spongaster tetras*	4.17	2
LO	*Dictyophimus inflatus*	4.2	1
LO	*Didymocyrtis penultima*	4.2	2
FO	*Pterocanium prismatium*	4.76	2
LO	*Stichocorys peregrina***	5.0	1
LO	*Solenosphaera omnitubus*	5.4	2
FO	*Dictyophimus inflatus*	5.6	1
LO	*Siphostichartus corona*	5.76	2
FO	*Sphaeropyle langii*	5.8/6.0	1
LO	*Dictyophimus splendens*	5.9	1
LO	*Theocorys redondoensis*	5.75/6.7	1
LO	*Lychnocanoma n. nipponica*	6.25	1
LO	*Stichocorys johnsoni*	6.34	2
LO	*Calocycletta caepa*	6.42	2
FO	*Lamprocyrtis heteroporos***	6.6	1
	*S. delmontensis –> S. peregrina**	6.66	2
FO	*Solenosphaera omnitubus*	7.2	2
	*S. delmontensis –> S. peregrina***	7.55	1
LO	*Amphymenium amphistylium*	7.55	1
LO	*Prunopyle hayesi*	7.6	1
LO	*Diartus hughesi*	7.67	2
FO	*Stylacontarium acquilonium*	7.7	1
LO	*Botryostrobus miralestensis*	8.21	2
LO	*Diartus petterssoni*	8.43	2
	D. petterssoni –> D. hughesi	8.7	2
LO	*Lychnocanoma n. magnacornuta*	8.8	1
FO	*Diartus hughesi*	8.89	2
LO	*Stichocorys wolffii*	8.89	2
LO	*Cyrtocapsella japonica***	10.0	1
LO	*Cyrtocapsella japonica**	10.09	2
LO	*Lithopera thornburgi*	10.09	2
LO	*Cyrtocapsella tetrapera*	10.9	1
LO	*Eucyrtidium inflatum*	10.9	1
LO	*Carpocanopsis cristata*	10.68	2
LO	*Cyrtocapsella cornuta*	11.8	1, 2
LO	*Lithopera renzae*	11.8	1, 2
LO	*Dorcadospyris alata*	11.86	2
FO	*Didymocyrtis petterssoni*	11.86	2
FO	*Cyrtocapsella japonica*	12.39	2
FO	*Lychnocanoma n. nipponica*	12.5	1
FO	*Lithopera thornburgi*	13.32	2
FO	*Calocycletta caepa*	13.35	2
LO	*Stichocorys armata*	13.72	2
LO	*Liriospyris parkerae*	14.46	2
LO	*Acrocubus octopyle*	14.55	2
LO	*Carpocanopsis bramlettei*	14.75	2
FO	*Stichocorys delmontensis***	14.9	1
LO	*Eucyrtidium asanoi*	14.9	1
FO	*Calocycletta costata*	15.12	2
FO	*Dictyophimus splendens*	15.5	1
FO	*Eucyrtidium inflatum*	15.5	1
LO	*Corythospyris?* sp.	15.5	1
	D. dentata –> D. alata	15.69	2
FO	*Lychnocanoma n. nipponica*	15.7	1
LO	*Liriospyris stauropora*	15.81	2
FO	*Liriospyris parkerae*	15.82	2
FO	*Eucyrtidium asanoi*	15.9	1
LO	*Eucyrtidium raphanes*	15.95	2
FO	*Carpocanopsis bramlettei*	16.08	2
FO	*Theocorys redondoensis*	16.25	1
LO	*Carpocanopsis cingulata*	16.44	2
FO	*Giraffospyris toxaria*	16.59	2
LO	*Didymocyrtis prismatica*	16.68	2
FO	*Corythospyris?* sp.	16.75	1
LO	*Cenosphaera* sp.	16.75	1
FO	*Lithopera renzae*	16.9	1
FO	*Cycladophora c. cosma*	17.2	1

Note: * = in the tropical eastern Pacific, ** = in the middle to North Pacific. Sources are based on the estimates published by (1) Morley and Nigrini (1995) for the middle to North Pacific, and (2) Shackleton et al. (1995) for the tropical eastern Pacific.

similar to those used to construct composite depth sections during previous ODP Legs (e.g., Leg 138; Hagelberg, Shackleton, Pisias, et al., 1992).

At each site, high-resolution (2- to 12-cm interval) measurements of magnetic susceptibility, GRAPE wet-bulk density, natural gamma-ray emissions, and *P*-wave velocity were made on the MST soon after the cores were retrieved and equilibrated to room temperature. These measurements were entered into the shipboard database. Additionally, measurements of color reflectance were made at 4- to 8-cm resolution on the split cores (see "Physical Properties" section, this chapter). Using GRAPE wet-bulk density, magnetic susceptibility, and color reflectance (450–500 or 650–700 nm band) as the primary lithologic parameters, the measurements from each hole were visually and quantitatively compared to determine if coring offsets were maintained between holes. Correlating events in multiple holes verified the extent of recovery of the sedimentary sequence. The use of at least two different physical properties allowed hole-to-hole correlations to be made with greater confidence than would be possible with only a single parameter.

Hole-to-hole correlations were made using interactive software developed specifically for this task. We used a software package called SPLICER that was developed at Lamont-Doherty Earth Observatory, patterned after the Leg 138 core-correlation software. Corresponding features in the data from cores in adjacent holes were aligned using both graphical and quantitative cross-correlations. Correlative features were aligned by adjusting the ODP meters below seafloor (mbsf) depths for a given core, on a core-by-core basis. No depths within a given core were adjusted. Multiple lithologic parameters were integrated to resolve discrepancies. The resulting adjusted depth scale is the meters composite depth (mcd) scale.

The need for adjustments to the shipboard mbsf depth scale arises from several sources. There is expansion of the sediment following core recovery, caused by the release of overburden pressure. Additionally, ship motion and heave may cause errors in the "true" in situ depth of each core. Thus, there are sections of missing sediment between cores even when core recovery is 100%. Also, the composite depth scale (mcd) is typically "stretched" by 10% relative to the mbsf scale.

Stretching and compression of the sedimentary features in aligned cores may also occur within cores. Because of distortion within individual cores, it was not possible to align every feature in the MST and color reflectance records accurately by simply adding a constant to the mbsf core depth. Within-core scale changes require postcruise processing to align smaller sedimentary features. Only after variable adjustments of peaks within each core can an accurate estimate of core gaps be made.

Figure 10 illustrates the need for hole-to-hole correlation and the mcd scale. In the left panel, color reflectance records from two holes are given on the mbsf depth scale. In the right panel, the same records are shown after depth scale adjustment. After adjusting the depth

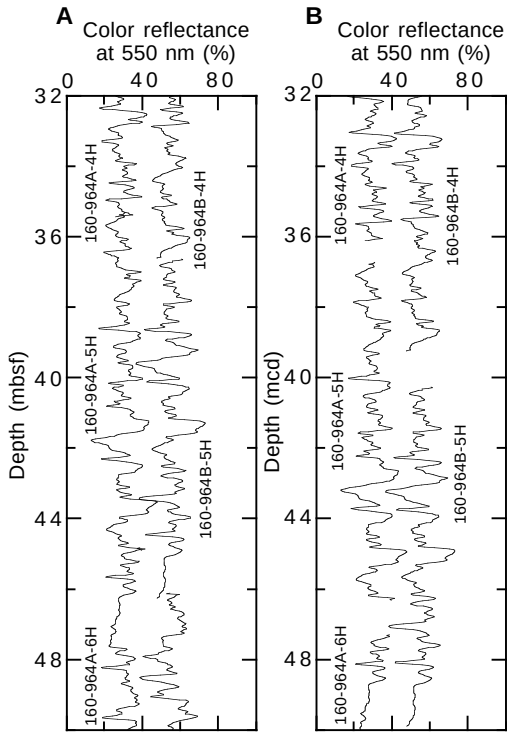

Figure 10. Portions of color reflectance records. The data from each hole are offset for clarity. **A.** Cores plotted on the ODP mbsf scale. **B.** The same cores in meters composite depth (mcd) scale. The composite depth section has the advantage that features common to all holes are in relative alignment.

scale so that features common to cores in all holes are aligned, coring gaps are obvious.

The correlation process was iterative. Records of a single physical parameter were moved along a depth scale, core by core, as correlations between the two holes were made. Although core distortion within a given core was, in some cases, significant, the core depths were only adjusted by a single constant for each core. The amount of adjustment necessary to optimize the correlation among multiple holes was retained for each core in each hole. The same process was then repeated for the other lithologic parameters to check the core adjustments. Where the amount of offset necessary to align features was ambiguous or uncertain even when using more than one lithologic parameter, or where multiple hole data were unavailable, no depth adjustment for that particular core was made. In these cases, the total amount of offset between mbsf depth and mcd is equal to the cumulative offsets from the overlying cores. When complete, confirmation of the composite depth section was provided by comparison with biostratigraphic data from multiple holes.

The composite depth section for each site is presented in tabular format. The composite depth table of Site 1019 is given as an example in Table 8. For each core, the last two columns in Table 8 give the depth offset applied to the ODP sub-bottom depth and the composite depth (in mcd), respectively. The offset column facilitates conversion of samples that are recorded in ODP sub-bottom depths to composite section depth. By adding the amount of offset listed in the table to the ODP sub-bottom depth (mbsf depth) of a measurement taken in a particular core, the equivalent in mcd is obtained. Thus, the depth conversion table can serve as a sampling strategy guide.

After composite depth construction, a single spliced record that was representative of the multiple-cored sedimentary sequence was assembled. The missing intervals of the sedimentary sequence that occur between successive cores of one hole could be patched with data from adjacent holes. By identifying the intervals where features present in the multiple holes were most highly correlated, it was possible to construct a spliced record without the danger of mistakenly duplicating any individual features or cycles. The resulting "splice" provides a single representative record of each physical property parameter (i.e., susceptibility, color reflectance, natural gamma ray, GRAPE) for a given site. Additionally, these single records are ideally suited to serve as sampling schemes for high-resolution paleoceanographic studies.

An example of a spliced magnetic susceptibility record is given in Figure 11. The left panel shows a spliced magnetic susceptibility record. The right panel shows the composite hole data used to con-

Table 8. Site 1019 composite depth section.

Core, section	Depth (mbsf)	Offset (m)	Depth (mcd)
167-1019A-			
1H-1	0.00	2.41	2.41
167-1019B-			
1H-1	0.00	7.37	7.37
167-1019C-			
1H-1	0.00	0.00	0.00
2H-1	8.30	0.01	8.31
3H-1	17.80	0.12	17.92
4H-1	27.30	2.12	29.42
5H-1	36.80	3.09	39.89
6H-1	46.30	1.51	47.81
7H-1	55.80	1.48	57.28
8H-1	65.30	1.70	67.00
9X-1	74.80	3.86	78.66
10X-1	84.50	2.94	87.44
11X-1	94.10	2.94	97.04
12X-1	103.70	2.94	106.64
13X-1	113.30	2.94	116.24
14X-1	122.90	4.88	127.78
15X-1	132.50	5.70	138.20
16X-1	142.10	4.72	146.82
17X-1	151.70	1.68	153.38
18X-1	161.30	3.30	164.60
19X-1	170.90	3.30	174.20
20X-1	180.50	3.30	183.80
21X-1	190.10	3.30	193.40
22X-1	199.70	3.30	203.00
23X-1	209.30	3.30	212.60
24X-1	219.00	3.30	222.30
25X-1	228.60	3.30	231.90
26X-1	238.20	3.30	241.50
167-1019D-			
1H-1	0.00	0.00	0.00
2H-1	3.60	0.83	4.43
3H-1	13.10	1.63	14.73
4H-1	22.60	2.92	25.52
5H-1	32.10	4.82	36.92
6H-1	41.60	7.09	48.69
7H-1	51.10	5.12	56.22
8X-1	60.60	5.12	65.72
9X-1	70.10	6.48	76.58
10X-1	79.60	6.48	86.08
11X-1	89.20	6.48	95.68
12X-1	98.90	6.48	105.38
13X-1	108.50	6.48	114.98
14X-1	118.10	6.48	124.58
15X-1	127.70	6.48	134.18
16X-1	137.30	6.48	143.78
18X-1	156.50	6.48	162.98
19X-2	166.62	6.48	173.10
20X-1	175.70	6.48	182.18
21X-1	185.30	6.48	191.78
22X-1	194.90	6.48	201.38
23X-1	204.50	6.48	210.98
24X-1	214.20	6.48	220.68
167-1019E-			
1H-1	0.00	0.00	0.00
2H-1	5.00	–0.10	4.90
3H-1	14.50	0.27	14.77
4H-1	24.00	0.98	24.98
5H-1	33.50	1.09	34.59
6H-1	43.00	1.35	44.35
7H-2	53.03	1.43	54.46
8H-1	62.00	0.86	62.86
9H-1	71.50	4.72	76.22
10H-1	81.00	4.72	85.72
11H-1	90.50	4.72	95.22
12H-1	100.00	5.62	105.62

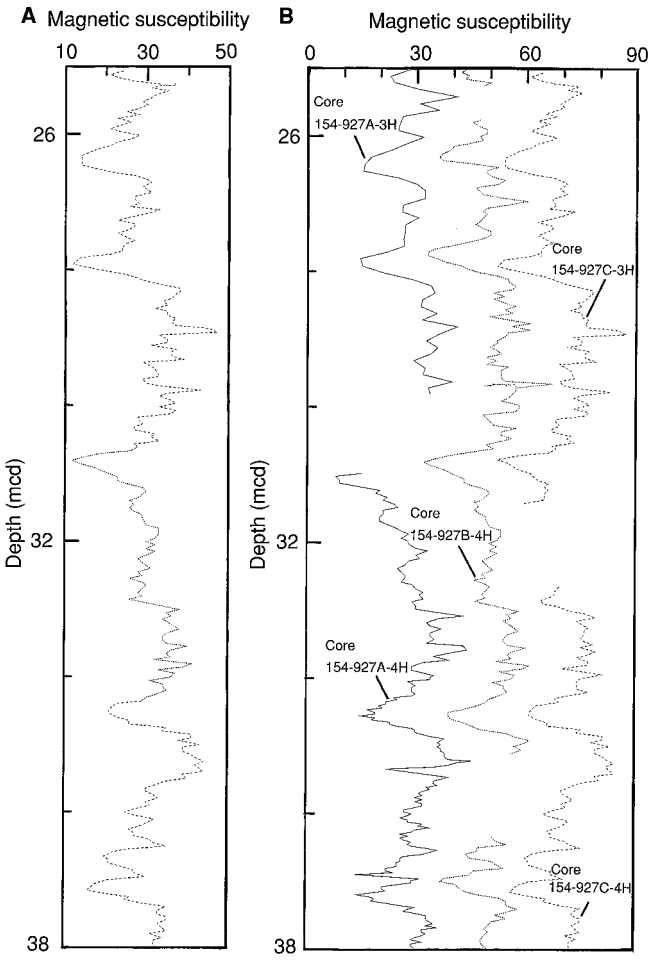

Figure 11. **A.** Portion of the spliced magnetic susceptibility record. **B.** Composite core data from the multiple holes. Data are offset for clarity.

Table 9. Site 1019 splice tie points.

Hole	Core, section, interval (cm)	Depth (mbsf)	Depth (mcd)		Hole	Core, section, interval (cm)	Depth (mbsf)	Depth (mcd)
1019C	1H-5, 123	7.23	7.23	tie to	1019E	2H-2, 83	7.33	7.23
1019E	2H-7, 47	14.47	14.37	tie to	1019C	2H-5, 6	14.36	14.37
1019C	2H-7, 11	16.91	16.92	tie to	1019E	3H-2, 65	16.65	16.92
1019E	3H-7, 7	23.75	24.02	tie to	1019C	3H-5, 10	23.90	24.02
1019C	3H-6, 63	25.93	26.05	tie to	1019E	4H-1, 107	25.07	26.05
1019E	4H-6, 139	32.89	33.87	tie to	1019C	4H-3, 145	31.75	33.87
1019C	4H-5, 139	34.69	36.81	tie to	1019E	5H-2, 72	35.72	36.81
1019E	5H-5, 35	39.85	40.94	tie to	1019C	5H-1, 105	37.85	40.94
1019C	5H-5, 119	43.99	47.08	tie to	1019E	6H-2, 123	45.73	47.08
1019E	6H-4, 19	47.69	49.04	tie to	1019C	6H-1, 143	47.53	49.04
1019C	6H-6, 83	54.34	55.85	tie to	1019E	7H-2, 139	54.42	55.85
1019E	7H-7, 35	60.88	62.31	tie to	1019C	7H-5, 1	60.83	62.31
1019C	7H-7, 135	65.17	66.65	tie to	1019E	8H-3, 79	65.79	66.65
1019E	8H-6, 139	70.89	71.75	tie to	1019C	8H-4, 131	70.05	71.75
1019C	8H-8, 51	75.25	76.95	tie to	1019E	9H-1, 873	72.18	76.95
1019E	9H-7, 75	81.25	85.97					

struct the splice. Tables that give the tie points for construction of the spliced record are given in each site chapter. An example of a table that provides tie points for the spliced records is shown in Table 9. The tie points can also be used to design a sampling strategy that will provide continuous records for high-resolution paleoceanographic studies. Typically, one hole at each site is chosen as a "backbone" for the record. The table indicates where tie points to other holes occur, and thus where sampling of other holes would provide data to fill the core gaps in the "backbone" record.

INORGANIC GEOCHEMISTRY

Interstitial Water Sampling and Chemistry

The interstitial water program used 5- to 10-cm-long whole-round sediment sections, which were cut and capped immediately after the cores arrived on deck. In one hole at each site, one whole-round sample was taken from each core for the first six cores and from every third core thereafter to total depth. Occasionally, samples from more than one hole were treated as constituting a single depth profile. At Site 1010, interstitial samples were taken more frequently in a dedicated hole (one/section for the first 50 m in Hole F), in addition to one/core for the first 10 cores in Hole C, for shore-based analyses of oxygen isotopes and deuterium. At Site 1019, interstitial samples were taken one/core throughout Hole 1019C. Before squeezing, samples were removed from the core liner and the outside surfaces were carefully scraped off with spatulas to minimize potential contamination. Whole rounds were placed into a titanium and stainless steel squeezing device and squeezed at ambient temperature with a hydraulic press. Interstitial water samples were collected in plastic syringes, filtered through 0.45-µm disposable filters, and stored in plastic sample bottles for shipboard analyses or archived in glass ampoules and/or heat-sealed plastic tubes for shore-based analyses.

Interstitial water analyses followed the procedures outlined by Gieskes et al. (1991). Interstitial water samples were analyzed for salinity with a hand-held refractometer; for pH and alkalinity by Gran titration with a Brinkman pH electrode and Metrohm autotitrator; for Cl^-, Ca^{2+}, and Mg^{2+} concentrations by titration; for SO_4^{2-} concentrations by ion chromatography with a Dionex DX-100 ion chromatograph; and for H_4SiO_4, HPO_4^{2-}, and NH_4^+ concentrations by spectrophotometric methods with a Milton Roy Spectronic 301 spectrophotometer; and for Li^+, Na^+, K^+, Sr^{2+}, and Mn^{2+} concentrations by flame spectrophotometric techniques with a Varian SpectrAA-20 atomic absorption spectrometer. International Association of Physical Sciences Organizations (IAPSO) standard seawater was used for calibrating techniques when applicable. The reproducibility of these techniques, expressed as 1σ standard deviations of means of multiple determinations of IAPSO standard seawater or of a standard treated as a sample, are alkalinity, 2%; Cl^-, 0.4%; Ca^{2+}, <1%; Mg^{2+}, 0.5%; SO_4^{2-}, 2%–3%; H_4SiO_4, 1%–3%; HPO_4^{2-}, 3%; NH_4^+, 2%–5%; and Li^+, Na^+, K^+, Sr^{2+}, and Mn^{2+}, 2%–4%. Na^+ was also determined with better precision by charge balance, neglecting contributions by ammonium, and these values are the ones reported. Chemical data for interstitial water are reported in molar concentration units in each site report.

ORGANIC GEOCHEMISTRY

The shipboard organic geochemistry program for Leg 167 included (1) real-time monitoring of volatile hydrocarbon gases, (2) measurement of the inorganic calcium carbon concentration to determine the amount of calcium carbonate in the sediments, (3) elemental analyses of total carbon and total nitrogen, (4) preliminary characterization of organic matter, and (5) analysis of long-chain alkenones. All methods and instruments used during Leg 167 are described below. Additional details are available in Emeis and Kvenvolden (1986). These analyses were made as a part of the routine shipboard safety requirements and to provide preliminary information for site summaries and shore-based organic geochemical research.

Hydrocarbon Gases: Sampling

During Leg 167, the compositions and concentrations of volatile hydrocarbons and other gases in the sediments were monitored at typical intervals of one per core. The headspace method was used throughout the cruise (Sites 1010–1022); gases released from the sediments after core recovery were analyzed by gas chromatography (GC) via the following technique. Immediately after retrieval on deck, a calibrated cork borer was used to obtain a measured volume of sediment from the end of one section of each core. The sediment sample, with a typical volume of approximately 5 cm^3, was placed in a 21.5-cm^3 glass serum vial that was sealed with a septum and metal crimp cap. When consolidated or lithified samples were encountered, chips of material were placed in the vial and sealed. Prior to gas analysis, the vial was heated in an oven at 60°C for 30 min. A 5-cm^3 volume of the headspace gas was extracted from each vial using a standard glass syringe. The collected gas was analyzed by gas chromatography.

The vacutainer method of gas sampling was used when gas pockets or expansion voids were observed in cores as they arrived on deck. During this leg, a new method of taking vacutainer gas samples was employed, using 50-mL syringes and small three-way stopcock valves. This new method saved time, yielded more sample volume, and allowed more control of samples than the previous method. A specially designed piercing tool equipped with a valve and needle was used to penetrate the core liner to transfer gas from the core to the syringe.

Hydrocarbon and Other Gases: Analysis

Headspace and vacutainer gas samples were both analyzed using a Hewlett-Packard 5890 II Plus gas chromatograph equipped with a 2.4 m × 3.2 mm stainless steel column, packed with HaySep S (80/100 mesh), and a flame ionization detector (FID). This instrument quickly measures the concentrations of methane, ethane, ethene, propane, and propene. Either the vacutainer or headspace syringe was directly connected to the gas chromatograph via a 1.0-cm^3 sample loop. Helium was used as the carrier gas, and the GC oven temperature was held at 90°C. Data were collected and evaluated with a Hewlett-Packard 3365 Chemstation data-handling program. Calibrations were done using Scotty IV analyzed gases, and gas concentrations were measured in ppm.

When higher concentrations of C_{2+} hydrocarbons were suspected, gas samples were analyzed with the Natural Gas Analyzer (NGA), which routinely measures hydrocarbons through C_6. This system consists of a Hewlett-Packard 5890 II Plus gas chromatograph equipped with a 60 m × 0.32 mm DB-1 capillary column and a flame ionization detector (FID). Non-hydrocarbon gases (N_2, O_2, CO_2, and H_2S) were analyzed at the same time by using a packed column and a thermal conductivity detector (TCD). For hydrocarbon analysis, the GC oven was heated at 40°C for 10 min and then ramped to 80°C at 4°C/min, yielding a total analysis time of 20 min. Helium was the carrier gas, and a Hewlett Packard Chemstation was used for data acquisition and processing. Chromatographic response was calibrated against pre-analyzed standards; gas contents are reported in ppm.

Inorganic Carbon

Carbonate carbon concentrations were determined using a Coulometrics 5011 carbon-dioxide coulometer. Routinely, one carbonate determination was performed for each 1.5-m section of core. A sample of approximately 30 mg of freeze-dried, ground sediment was reacted with 2N HCl. The liberated CO_2 was back-titrated to a colorimetric endpoint. Percentage of carbonate is calculated from the inorganic carbon (IC) content with the assumption that all inorganic carbon is present as calcium carbonate

$$CaCO_3 = IC \cdot 8.33.$$

Elemental Analyses

Total carbon, total nitrogen, and total sulfur were determined using a Carlo Erba 1500 CN Analyzer. Approximately 10 mg of freeze-dried, ground sediment was combusted at 1000°C in a stream of oxygen. Using helium as a carrier gas, the oxygen was removed and the combustion products were reduced. The reduced gases were separated by gas chromatography and quantified with a TCD. Contents of total organic carbon (TOC) were calculated as the difference between total carbon (TC) and inorganic carbon (IC)

$$TOC = TC - IC.$$

Organic Matter Characterization and Determination of Maturity

The type of organic matter was also characterized in a selected set of samples by pyrolysis using a Delsi Nermag Rock-Eval II system. This method is based on a whole-rock pyrolysis technique designed to identify the type and maturity of organic matter and to detect the petroleum potential of the sediments (Tissot and Welte, 1984; Espitalié et al., 1986). The Rock-Eval system includes a temperature program that first releases volatile hydrocarbons (S_1) at 300°C for 3 min. Hydrocarbons are then released through thermal cracking of kerogen (S_2) as the temperature is increased from 300°C to 550°C at 25°C/min. S_1 and S_2 hydrocarbons are measured with a FID and reported in milligrams per gram of sediment. The temperature at which the kerogen yields the maximum amount of hydrocarbon during the S_2 program provides T_{max}, a parameter used to assess the maturity of the organic matter. Between 300°C and 390°C of the stepped pyrolysis, CO_2 released from the thermal degradation of organic matter (S_3) is trapped and measured by a TCD in milligrams per gram of sediment. Rock-Eval II parameters help in characterizing organic matter by allowing the following indices to be calculated: Hydrogen Index (HI; $100 \cdot S_2/TOC$), Oxygen Index (OI; $100 \cdot S_3/TOC$), S_2/S_3 ratio, and Production Index (PI; $S_1/(S_1+S_2)$). Interpretation of Rock-Eval data is considered to be compromised for samples containing less than 0.5% TOC (Peters, 1986).

Analysis of Long-Chain Alkenones

Long-chain alkenones were analyzed for sediments younger than 270 ka from Sites 1017 and 1019 to estimate paleo-sea-surface temperature (SST). Solvent extract (bitumen) was obtained from 1 g of freeze-dried sediment by ultrasonic extraction with dichloromethane methanol (99/1) for 30 min. The supernatant was pipetted into a vial, and the solvent was removed under a stream of nitrogen. The total extract was dissolved in 50 µL of hexane, and a 1-µL aliquot was then analyzed by gas chromatography on a Hewlett-Packard Model 5890 II gas chromatograph, equipped with a 50 m × 0.2 mm HP Ultra 1 (Cross Linked Methyl Silicon Gum) capillary column (0.11 µm film thickness). Operating conditions were as follows: splitless injection; injector, 300°C; detector, 320°C; temperature program, 50°C (2 min), 20°C/min to 130°C, 4°C/min to 320°C (hold 20 min), 70°C/min to 50°C. Identification of alkenones was based on comparison of retention sequences with those in published literature (e.g., Brassell et al., 1986; Prahl and Wakeham, 1987; Prell, Niitsuma, et al., 1989). The degrees of unsaturation of C_{37} alkenones (U^k_{37} and $U^k_{37}{}'$ indices), which reflect sea-surface temperature (SST), are calculated as $U^k_{37} = (C_{37:2} - C_{37:4}) / (C_{37:2} + C_{37:3} + C_{37:4})$ and $U^k_{37}{}' = C_{37:2} / (C_{37:2} + C_{37:3})$, respectively. Since the identification of $C_{37:4}$ alkenone was impossible because of the lack of a standard and/or a gas chromatograph-mass spectrometer, $U^k_{37}{}'$ was used in this study. The calculation of

SST was conducted according to the equation $U^{k}_{37}' = 0.034$ SST + 0.039, based on an experimental result for cultured *Emiliania huxleyi* (Prahl et al., 1988) with an estimated analytical accuracy of 0.5% (Prahl and Wakeham, 1987).

PHYSICAL PROPERTIES

Introduction

Physical properties were measured for three main purposes: (1) to provide near-continuous records for hole-to-hole correlation, the construction of complete stratigraphic sequences, and core-to-downhole log ties; (2) to provide estimates of properties related to composition and consolidation history of the sediments, such as porosity, natural gamma radiation, magnetic susceptibility, and color reflectance; and (3) to furnish data for the calculation of synthetic seismograms *(P*-wave velocity and bulk density), for the estimation of mass accumulation rates (dry-bulk density), and for the calculation of local heat flow (thermal conductivity).

The first measurement station was the multisensor track (MST). Four sensors on an automated track nondestructively measure bulk density, magnetic susceptibility, natural gamma-ray emission, and *P*-wave velocity on whole-core sections. Next, thermal conductivity was measured on whole-core sections. The cores were then split. The archive half was used for nondestructive measurements of color reflectance and for recording color digital images. The working half was measured for further *P*-wave velocity and sampled for further gravimetric determination of index properties. The methods used to measure and calculate these properties are described in the following sections.

Index Properties

Index properties, as defined for ODP shipboard procedures, include gravimetric determinations of water content, bulk density, grain (solid) density, and related properties such as porosity, void ratio, and dry density. The first measured parameter was initial wet-bulk mass (M_b). Dry mass (M_d) and volume (V_d) were measured after drying the samples in a convection oven for 24 hr at temperatures varying from 95°C to 105°C. All calculations, including the salt correction, which accounts for the pore-water salt left in the sample during drying, were performed by the shipboard IP/4D program using Method C and are summarized below. The program code is appended to the shipboard laboratory manual for index properties.

Salt corrections on M_d and V_d are performed using the evaporated mass of pure water (M_w), salinity (s) = 0.035, corresponding pore-water density (ρ_{pw}) = 1.024 g/cm^3, and salt density (ρ_{salt}) = 2.257 g/cm^3. The mass of salt is

$$M_{salt} = M_w \cdot s/(1-s) \quad (1)$$

It follows, therefore, that corrected pore-water mass (M_{pw}), pore-water volume (V_{pw}), solid mass (M_s), and solid volume (V_s) are, respectively

$$M_{pw} = M_w + M_{salt} = M_w/(1-s) \quad (2)$$

$$V_{pw} = M_{pw}/\rho_{pw} \quad (3)$$

$$M_s = M_d - M_{salt} \quad (4)$$

$$V_s = V_d - V_{salt} = V_d - M_{salt}/\rho_{salt} \quad (5)$$

Water content can be expressed as a ratio of M_{pw} to either M_s (as W_s) or bulk mass M_b (as W_b)

$$W_s = M_{pw}/M_s = (M_b - M_d)/(M_d - sM_b) \quad (6)$$

$$W_b = M_{pw}/M_b = (M_b - M_d)/[(1-s)M_b] \quad (7)$$

Water content is often referred to as "% dry mass of sample" ($W_s \cdot 100\%$) or "% wet mass of sample" ($W_b \cdot 100\%$) (see also ASTM standard D 2216-80; ASTM, 1980). Grain (solid) density (ρ_s) and bulk density (ρ_b) are then calculated as

$$\rho_s = M_s/V_s \quad (8)$$

$$\rho_b = (M_s + M_{pw})/(V_s + V_{pw}) \quad (9)$$

Porosity (Φ) and void ratio (e) are volumetric, relative expressions of water content, assuming that all original sediment voids are represented by pore water in the recovered cores. Note that gas that in situ is free or in solution partly escapes during core recovery and almost completely disappears from the voids when the cores are sectioned and split; therefore, gas is not quantified by gravimetric methods, which assume water saturation. Porosity and void ratio are respectively calculated as

$$\Phi = V_v/V_b = W_b \cdot \rho_b/\rho_{pw} \quad (10)$$

$$e = V_v/V_s = W_s \cdot \rho_s/\rho_{pw} \quad (11)$$

Dry density (ρ_d) is used to estimate the mass accumulation rate for a given depth interval and is defined as

$$\rho_d = M_s/V_b = \rho_b \cdot W_b/W_s \quad (12)$$

Samples for index properties measurements were taken at an average frequency of one per core section. However, where frequent lithological changes occurred, more dense sampling was undertaken to ensure measurements from all significant lithologies throughout the core.

The samples for index properties measurements were generally taken within a few centimeters of the position for measurements of *P*-wave velocity (see below), and adjacent to the color reflectance measurement (see below) and where the carbonate sample was taken (see "Organic Geochemistry" section, this chapter). This ensured that the different parameters represent the same sediment type, and, therefore, can be correlated without interpolation. In XCB cores, which frequently showed "biscuiting" disturbance, particular care was taken to sample undisturbed parts of the core sections and to avoid the drilling slurry.

Mass determinations were precise to within ±0.005 g (<0.5%) and volume determination to within ±0.02 g/cm^3 (<1%). Balance and pycnometer precision are estimated from control measurements run routinely on mass standards and a calibration cylinder of known volume. Pycnometer calibrations were performed when measured value of the standard was off by more than ±0.02 g/cm^3 from the known value. The total standard error for index properties is estimated to be less than 2%. This precision estimate is unrelated to potential deviations from in situ values or to the accuracy of the result.

Bulk Density (Gamma-Ray Attenuation)

An additional estimate of bulk density was obtained from logging of whole-round core sections with the Gamma-Ray Attenuation Porosity Evaluator (GRAPE). This device measures the electron density (ρ_e), which is related logarithmically to the gamma-ray attenuation by

$$\rho_e = 1/\mu d \cdot \ln(N_0/N) \quad (13)$$

where μ is the gamma-ray attenuation coefficient, d the thickness of the sample (maximum core diameter), N_0 the incident gamma-ray intensity, and N the detected gamma-ray intensity after attenuation. For a certain range of electron energies caused largely by Compton scattering (about 0.2 – 2.0 MeV), the electron density is related to the bulk density ρ_b by

$$\rho_e = \rho_b (Z/A) N_A \quad (14)$$

where Z is the atomic number, A the atomic mass, and N_A Avogadro's number. Because Z/A is about 0.5 for all common minerals, the bulk density of minerals can be accurately measured from the gamma-ray intensity ratio N_0/N, using a calibration based on aluminum standards of different thicknesses. Z/A is about 1 for water, however, and a correction based on a porosity evaluation is therefore applied to the first approximation of ρ_b (reported as GRAPE density) to get a more realistic corrected GRAPE density. GRAPE density measurements were generally taken at 4-cm intervals.

Natural Gamma-Ray Emission

Natural gamma-ray measurements were generally taken on the MST for periods of 15 s every 12 cm while the core was stopped. At the beginning of the leg, a calibration was performed using potassium and thorium standards, and background radiation was determined with a water core to be about 8–9 cps. The total counts were useful for defining some lithologic trends, core-log ties, and is a secondary tool for composite section construction. The relatively short sampling period of 15 s does not allow for the accumulation of sufficient counts to measure elemental abundances with the five energy windows acquired routinely by the MST program.

Magnetic Susceptibility

Magnetic susceptibility was measured on the MST with the Bartington susceptibility meter MS1 using a 8-cm loop at low sensitivity (1 s measuring time). Sample periods were 4 s and sample intervals 4 cm. Magnetic susceptibility, GRAPE, and color reflectance were the most useful records for core-to-core correlation and composite depth construction.

Velocity

P-wave velocity was generally measured at 4-cm intervals on whole-round core sections, orthogonal to the core axis (x- and y-directions), with the *P*-wave logger (PWL) mounted on the MST. In addition, *P*-wave velocity was measured on split-core sections using the three different transducer pairs of the digital sound velocimeter. Pair T1 was inserted along the core axis (z-direction) and pair T2 was inserted orthogonal to the core axis (y-direction; Fig. 12). Pairs T1 and T2 were used for soft sediments. Pair T1 and pair T2 are the same transducer type, mounted with fixed separations, approximately 7.0 cm for T1 and 3.5 cm for T2. Pair T3 (modified Hamilton frame), used for more lithified sediments, measured either across the split-core section and core liner orthogonal to the core axis (x-direction) through transducer contact with the sediment on top and the core liner on bottom or through pieces of more indurated core removed from the liner with core-axis orientation as noted in the data tables. The signal used for all transducer pairs is a 0.1 μs square wave with a period of 0.2 ms. The received signal was stacked on the rise of the source impulse, resulting in decreased noise and improved detection of the first arrival. The first arrivals were hand picked and the VSR software calculated sediment velocity. All *P*-wave source and receiver frequencies were 500 kHz. The T1 and T2 split-core velocimeters calculate velocity based on a fixed distance and measured travel time. In addition to travel time, the T3 system measures variable sample thickness with a digital micrometer and monitors pressure exerted on sediments by the transducer pair.

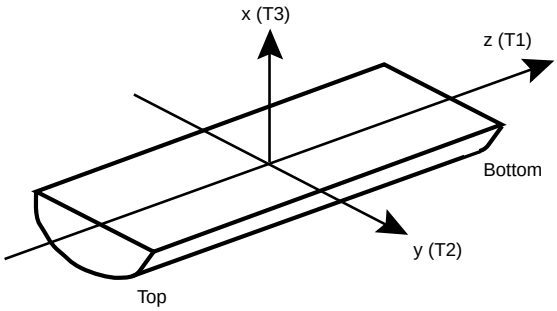

Figure 12. Diagram of discrete *P*-wave velocity measurement directions with respect to the orientation of the working-half section of core.

The PWL was calibrated at the beginning of the leg. A four-point calibration was conducted for the displacement transducer using acrylic cylinders of varying diameters. The displacement transducer measures the core thickness and uses this measure to calculate *P*-wave velocity in the sediments, integrating over intervals of 4 cm. As a velocity control, the water standard was run and a correction factor compensating for velocity in the liner and electronic delay was adjusted to give the expected theoretical velocity in water at laboratory temperature. Reported velocities are not temperature-corrected.

Spectral Reflectance

The Oregon State University spectral reflectometer was used to make systematic measurements of the relative spectral reflectance of the sediments. The instrument consists of a computer-controlled, motorized track assembly that advances a core section into sampling position under a commercially available light integration sphere. The integration sphere is brought into contact with the sediment via a computer-controlled, vertical stepping motor. Temperature, conductivity, and strain sensors detect contact with the sediment surface. Light with known spectral characteristics passing through fiber optics is steered using a directional mirror toward two reference ports and a sample port during each measurement. The light that is diffusely reflected off the sediments is integrated within the sphere and then split into constituent wavelengths by a diffraction grating and collected with a 1024-channel spectrometer.

The instrument used during Leg 167 was the same as that used on Leg 162 (see Shipboard Scientific Party, 1996), with three notable improvements: (1) a spring-loaded device that mounts the sphere to the vertical lander, (2) an externally mounted temperature control for the spectrometer, and (3) a software option to measure internal "black" background every third sample. The first modification has improved sphere/sample contact, thereby minimizing light loss. The second has reduced background light energy caused by heat, improving the signal-to-noise ratio across the entire spectrum. The third has decreased run time without compromising data quality. Analyses of sample and standard runs shows stable background levels within and between different core sections.

Reflected light was measured in 1024 0.628-nm-wide bands ranging from 250–950 nm. These measurements were taken at 6-cm intervals, on average, on all APC and some XCB cores from the first two holes at each site, and on chosen intervals from the other holes. For shipboard analysis, the raw data was converted to percent reflectance and averaged into four 50-nm-wide bands defined as ultraviolet (UV; 250–300 nm), blue (450–500 nm), red (650–700 nm), and near infrared (nIr; 850–900 nm). We employed the red and blue bands, which are near the instrument's maximum response, as an aid in defining lithostratigraphic units. These bands were also used when con-

structing composite sections (see "Composite Depths" section, this chapter). Prior to Leg 167, regression equations relating reflectance to opal, organic carbon, and carbonate were generated using data from EW9504 Site Survey piston cores. Regression equations were also generated during Leg 167 using carbonate data produced on board. These equations and reflectance data were used to make high-resolution predictions of calcium carbonate and opal content in real-time aboard ship.

Digital Imaging

Using the ODP color digital imaging system, each 20-cm interval of core was captured in a rectangular (1008 pixels long by 486 pixels wide) 24-bit color image. Coverage of each pixel is 0.25 mm, measured down the core.

The system differs from the SONY DXC-750MD camera-based system described by Merrill and Beck (1995); it is more automated and filtered tungsten lamps have been replaced by 200-watt daylight-balanced Hydrargyrum Medium Arc Iodide (HMI) lamps. HMI lamps are more stable than filtered tungsten lamps, with an initial color temperature of 5600 K that decreases at a rate of ~1 K/hr of use. The age of each pair of bulbs was metered, so they could be replaced when their color temperature dropped below 4700 K.

Using the ODP color system (v 3.01) software, color value measurements were made at 1.0-mm intervals in each image and then made into full core plots using an automated mosaic. Results are reported in the CIELAB color measurement system (Wyszecki and Stiles, 1982). The CIELAB a* axis represents the range of color values from green (negative values) to red (positive values) and the b* axis represent color values from blue (negative) to yellow (positive). Reported color values have been corrected for drift in color temperature and for observed non-uniformity in intensity of the illuminant. The latter correction has been accomplished by fitting a curve to values measured for a uniform gray target, noting the departure of that curve from that of an ideal flat illuminant, and applying the resulting correction to observations made on cores.

Thermal Conductivity

Thermal conductivity was measured using needle probes in full-space configuration. At the beginning of the leg, the instrument was calibrated to produce the heat in the needle specified in the shipboard TC/PC program that is used to calculate thermal conductivity. In addition, four standard materials: macor, 1.61 ± 0.1 W/(m·K); red rubber, 0.96 ± 0.1 W/(m·K); black rubber, 0.54 ± 0.05 W/(m·K); and gelatin, 0.67 ± 0.02 W/(m·K) were measured with seven needles used for core measurements. Average values for each standard were used to calculate regression coefficients (Table 10). The thermal conductivity measurements were normalized for different needle probes using the control measurements taken in the black rubber standard.

The data acquisition program performed a temperature drift study for each run and measurements were carried out when the cores had equilibrated to ambient temperature (about 3–4 hr after recovery). While the needle was heated, temperature T was measured with elapsed time t (every 30 s for 6 min) and related to the thermal conductivity of the sediment by

$$T = (q/4\pi k)\ln(t) + C \quad (15)$$

where q is heat input per unit time and unit length (W/m^2) and k is the thermal conductivity (W/m·K). Term C includes temperature drift during measurement as well as the non-linearity resulting from imperfections in the experiment. Equation (15) is solved for k by applying a least-squares fit to the T vs. t data. An interactive display allows the user to determine the time interval used in the fit. The interval was generally set between 60 and 240 s.

Table 10. Thermal conductivity standard measurements and regression coefficients used to correct raw measurements.

Standards	Known thermal conductivity	Measured thermal conductivity (W/[m·K])								
		Needle 339	Needle 352	Needle 355	Needle 361	Needle 362	Needle 364	Needle 365	Needle 366	Needle 367
Black Rubber	0.54	0.5814	0.5327	0.5524	0.4626	0.52895	0.5744	0.6018	0.5943	0.5621
		0.5629	0.5613	0.5447	0.4514	0.53568	0.5499	0.6084	0.5498	0.5446
		0.5716	0.544	0.5441	0.4514	0.5344	0.5248	0.6329	0.5798	0.5293
		0.5621	0.5076	0.5634	0.4226	0.51193	0.5286	0.6005	0.5922	0.5287
	Average	0.5695	0.5364	0.5512	0.4470	0.5277	0.5444	0.6109	0.5790	0.5412
	SE	0.0090	0.0225	0.0090	0.0171	0.0109	0.0228	0.0151	0.0205	0.0158
Red Rubber	0.96	1.1291	0.9834	1.0239	0.98427	1.0022	1.2285	1.0460		
		1.0563	1.0475	0.9970	0.9392	1.2500	1.0132	1.0907		
		1.0752	0.9779	0.9856	0.8717	0.8289	1.0438	0.9226		
		0.9781	0.9601	1.0127	0.9263	0.87387		1.0936		
	Average	1.0597	0.9922	1.0048	0.9304	0.9887	1.0952	1.0382		
	SE	0.0625	0.0382	0.0169	0.0463	0.1752	0.1522	0.0316		
Macor	1.61	1.9446	1.8428	1.6919	1.6421	1.5244	2.4076	2.4270	2.4270	2.3502
		2.0185	1.6035	1.9426	1.5075	1.5825	2.7582	2.7582	2.7582	2.4562
		2.0069	1.6804	1.6712	1.8274	1.7790	2.7135	2.7135	2.7135	2.0382
		1.9433	1.6283	1.6564	1.6044	1.5751	2.2988	2.6879	2.6879	1.9523
	Average	1.9783	1.6888	1.7405	1.6454	1.6153	2.5445	2.6466	2.6466	2.1992
	SE	0.0400	0.1076	0.1355	0.1340	0.1122	0.2261	0.1493	0.1493	0.2420
Gelatin	0.67	0.6249	0.7129	0.7588	0.7120	0.6418	0.8278	0.7812	0.9515	0.6782
		0.7302	0.7325	0.7035	0.6666	0.6375	0.9241	0.7865	0.8295	0.7297
		0.7552	0.7133	0.7468	0.6773	0.6337	0.8023	0.7969	0.8303	0.7695
		0.7328	0.7039	0.7514	0.6980	0.6679	0.9231	0.8140	0.8563	0.7196
	Average	0.7108	0.7156	0.7401	0.6885	0.6452	0.8693	0.7946	0.8669	0.7243
	SE	0.0583	0.0120	0.0249	0.0204	0.0155	0.0635	0.0144	0.0577	0.0375
Slope		0.74331	0.9409	0.9016	0.9064	0.0397	0.5094	0.5125	0.5150	0.6349
Intercept		0.14754	0.0202	0.0402	0.1091	0.9641	0.3328	0.2545	0.2441	0.2135
R^2		0.99938	0.9994	0.9984	0.9953	0.9989	0.9931	1.0000	0.9994	1.0000

Note: SE = standard error.

Downhole Temperature

Downhole temperature measurements using Adara tools followed the procedures and used the tools described by Fisher and Becker (1993). Convection from downhole or circulation from the drill string would mix the bottom water with warmer water. Bottom-water temperature, therefore, was chosen from the lowest recorded temperature while holding the tool ~0–20 m above mudline for up to 10 min before and/or after coring.

Heat Flow

Heat flow was determined at several sites using thermal conductivity measurements on whole-round core sections, and with downhole temperature measurements using the Adara temperature probe, which fits into the coring shoe of the APC barrel. One objective was to investigate the geothermal response to recent bottom-water temperature changes.

DOWNHOLE MEASUREMENTS

Introduction

After completing coring operations, the hole was flushed of debris and a series of separate toolstrings were lowered on a seven-conductor cable through the drillpipe and into the hole for downhole measurements of physical properties. A wireline heave motion compensator was employed during rough seas to reduce by half the effect of ship heave on the tool position in the borehole (Goldberg, 1990). The sensors continuously monitored geophysical or structural properties of the formation, which were typically recorded at 15-cm depth increments by the Schlumberger MAXIS 500 or Cyber Service Unit (CSU) computers. The in-formation depths of investigation and vertical resolutions are sensor-dependent but are typically between 30 to 60 cm.

Three different Schlumberger tool strings were used on Leg 167, the first of which is new to the program: (1) the density-porosity combination tool string, (2) the combined sonic-Formation MicroScanner (FMS) tool string, and (3) geological High-Sensitivity Magnetic Tool (GHMT). A schematic diagram of these tool strings is shown in Figure 13. The Lamont-Doherty temperature tool was attached to the base of each tool string to measure downhole temperature gradients.

Density-Porosity Combination Tool String

This tool string was first introduced to ODP during Leg 166 and consists of four main sensors: (1) the hostile-environment natural gamma-ray spectrometry tool (H-NGS), (2) the accelerator porosity sonde (APS), (3) the high-temperature lithodensity tool (HLDT), and (4) the phasor dual-induction tool (DIT). This new tool string presents significant improvements in gamma-ray and neutron porosity measurement sensitivity and vertical resolution. This tool string is designed to measure natural gamma-ray activity, formation porosity and atomic density, formation bulk density, hole diameter (caliper), and deep, intermediate, and shallow resistivity. The tool string was logged at 300 m/hr and data were collected at standard 15-cm sample rates, with additional higher sampling-rate records of bulk density (2.5 cm), porosity (5 cm), and resistivity (5 cm).

The DIT provides three measurements of electrical resistivity, all with different radial depths of investigation. Two induction devices ("deep" and "medium" resistivity) send high-frequency alternating current through transmitter coils, creating a magnetic field that induces a secondary (Foucault) current in the formation. This ground-loop current produces a new inductive signal, proportional to the conductivity of the formation. This inductive signal is recorded by a series of receiving coils and is then converted to resistivity values. A third

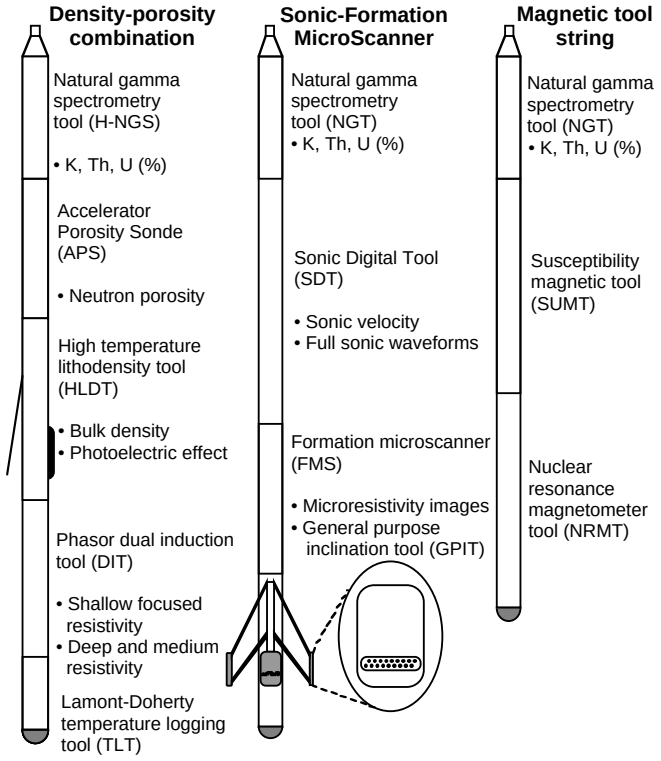

Figure 13. Schematic diagram of Schlumberger logging tool strings used on Leg 167. Tool strings are not drawn to relative scale.

device, the spherically focused resistivity tool (SFL), measures the current necessary to maintain a constant voltage drop across a fixed interval. Vertical resolution is 2 m for the deep induction, 1.5 m for the medium induction, and 0.75 m for the SFL. The data are corrected for irregularities in borehole diameter. Like the HLDT density tool, the induction resistivity tools can be run in high-resolution mode. Real-time phasor processing enhances the SFL tool's intrinsic resolution and sample density increases from 15 cm to 2.5 cm.

Resistivity varies as a function of the inverse square root of porosity (Archie, 1942). Fluid salinity, clay content, hydrocarbon content, and temperature also are important factors influencing electrical resistivity. Other factors that may affect the measured resistivity are the concentration of hydrous and metallic minerals, formation porosity, and the geometry of the pore space. The Leg 167 resistivity logs are mainly reflecting variations in sediment porosity associated with changes in sediment composition and burial compaction.

The HLDT utilizes a ^{137}Ce source of 0.66 MeV gamma rays for formation bulk-density measurement. The source is mounted in the tool body and an eccentralizing arm presses it and a pair of detectors against the borehole wall. Determination of density is based on the theory of Compton scattering of gamma rays within the formation, which is a function of electron density. The electron density is converted to bulk density on the assumption that most rock-forming elements have atomic weights that are twice their atomic numbers.

In addition, the lithodensity tool records a photoelectric effect index. Photoelectric absorption occurs in the energy window below 150 KeV and is principally dependent upon the energy of the incident gamma ray and the atomic cross section. The measurement is independent of porosity and therefore can be used as a matrix lithology indicator. The density and photoelectric effect measurements require good contact between the sensor and borehole wall; the tool measures the "standoff" and corrections can be made for excessive borehole roughness. The intrinsic vertical resolution of the tool is approxi-

mately 0.45 m, in agreement with a recent analysis of ODP core and log density data from Leg 138 (Harris et al., 1995).

The HLDT tool was run in high-resolution mode, which substantially improved counting statistics and measurement resolution. Logging speed must be reduced to 300 m/hr and the resulting data are processed real-time (alpha-processing) to take dual advantage of the near detector-source spacing (15 cm) and the far detector measurement stability. Sample interval was reduced from the standard 15 cm to 2.5 cm, and the intrinsic resolution approaches the near detector spacing (15 cm). Excellent hole conditions are a main prerequisite for high-resolution data reliability.

The APS uses an electronic neutron source (14 MeV) with one epithermal and four thermal detectors to measure hydrogen abundance which, in turn, is recalculated as porosity. Energy loss by incident high-energy neutrons depends largely on the concentration of hydrogen in the formation since the neutrons and hydrogen atoms have nearly equal mass. Within a few microseconds, the neutrons have been slowed down to thermal velocities and are captured by other atomic nuclei such as Si or Ca. The total hydrogen content of the formation is determined by the flux ratio of emitted to detected neutrons. Free water content (porosity) is determined from the thermal neutron counts. Water that is structurally bound (e.g., in clay minerals) can be estimated by subtracting free water from total water estimates. In contrast to the formerly used Compensated Neutron Tool (CNT), the APS was designed for enhanced sensitivity and thin-bed detection; resolution is approximately 30 cm.

Sonic-Formation MicroScanner Combination Tool String

The FMS produces high-resolution images of the microresistivity character of the borehole wall that can be used for detailed sedimentological and/or structural interpretations (Ekstrom et al., 1986). The FMS tool comprises 16 electrode "buttons" on four orthogonal pads that are pressed against the borehole wall. The electrodes are spaced approximately 2.5 mm apart and are arranged in two diagonally offset rows of eight electrodes each. Processing corrects the offset rows to one level, doubling the horizontal resolution to approximately 1.25 mm. The FMS tool string contains a general purpose inclinometry tool (GPIT) that orients the resistivity measurements through the use of an accelerometer and a magnetometer. The tool string includes a natural gamma-ray spectrometry tool (NGT) to enable correlation of the FMS to other tool strings. Using the new Maxis 500 logging unit the raw data are processed real-time during logging to transform individual microresistivity traces into complete, oriented images. Full-color images are available shortly after logging. Scientific applications of the FMS images include detailed correlation of coring and logging depths, core orientation, mapping of fractures, faults, foliations, and other formation structures, as well as determination of strikes and dips of bedding planes.

The sonic digital tool (SDT) records the time required for sound to travel along the borehole wall from one of two acoustic transmitters to two receivers over source-receiver distances of 2.4, 3.0, and 3.6 m. First arrivals for the individual source-receiver paths are used to calculate sonic velocities; four velocity values are measured at each depth, along four possible paths. Only compressional-wave velocities are determined on board ship; however, the full sonic waveforms are recorded for post-cruise processing to determine shear wave and Stonely wave velocities. Logs can be corrected for cycle skipping (where the receiver misses the first arrival and responds instead to the second signal) using the four-fold measurement redundancy. Compressional-wave velocity is controlled primarily by porosity and lithification; decreases in porosity and increases in consolidation and lithification typically result in velocity increases with depth in a sedimentary deposit.

The Lamont-Doherty Temperature Tool

The LDEO temperature logging tool (TLT) is a self-contained tool that can be attached to the base of any of the sensor combinations. Data from two thermistors and a pressure transducer are collected every 1 s and are recorded internally. Once the in situ measurement is completed, the data are transferred to a shipboard computer for analysis. The fast-response thermistor, though less accurate, is able to detect small, abrupt temperature excursions caused by fluid flow from the formation. The slow-response thermistor is more accurate and can be used to estimate the borehole temperature gradient. The TLT measures the borehole water temperature, not the true formation temperature, and, therefore, is an underestimate of temperature because of the cooling effect of sea water circulation during drilling. Data are recorded as a function of time, with conversion to depth (meters logging depth) achieved after logging using the MAXIS 500 wireline depth counter data.

Geological High-Sensitivity Magnetic Tool

High-sensitivity total magnetic field and susceptibility logging tools were deployed on Leg 167 to resolve borehole magnetic polarity transitions and magnetic susceptibility variations. The total magnetic field tool failed on Leg 167, but susceptibility logs were taken at most sites. Similar tools were run previously on Legs 134 and 145. These tools were developed jointly by oil industry (TOTAL and Schlumberger) and French government research institutions (CEA-LETI and CNRS-ENS). The tools were designed and constructed by a branch of the French Atomic Energy Commission (CEA-LETI), which also developed the analysis software.

Magnetic induction **B** in a borehole depends on location p and time t with (Pozzi et al., 1988):

$$\mathbf{B}(p,t) = \mathbf{Br}(p) + \mathbf{Ba}(p) + \mathbf{Bf}(p) + \mathbf{Bt}(p,t).$$

Br(p) is the regular inner field, whereas **Ba**(p) is the anomaly field related to large-scale heterogeneities in susceptibility or in magnetic remanence. In the absence of such heterogeneities, the spatial variation of both **Br** and **Bf** with depth is linear. **Bf**(p) is the induction caused by the magnetization (induced and remanent) of the sediments around the borehole and can easily be separated from **Br**(p) and **Ba**(p). **Bt**(p,t) is time dependent and represents the induction caused by transient variations of the Earth's field. The time-dependent component can be reduced using a radiolinked reference, or it can be estimated by repeat sections. To obtain direct magnetostratigraphy from **Bf**(p), the susceptibility and the total field measurements are combined to discriminate the induced and remanent magnetizations. Specifications of the probes such as impulse response, calibration ratio, and geomagnetic field direction at the hole are used to calculate the susceptibility effect on the scalar total field magnetometer. The result of calculations is the scalar remanent magnetization.

The Nuclear Resonance Magnetometer Tool (NRMT) can be used in borehole temperatures up to 125°C; however, the probe used for Leg 167 is more precise and has a maximum operating temperature of 65°C. Average precision of this tool is 0.5 nT based on repeat sections. The Susceptibility Magnetic Tool (SUMT) employs a classic measurement principal that detects the mutual induction signal between two coils (0.8 m apart) caused by the surrounding borehole lithology. The excitation frequency is about 200 Hz. The precision be-

tween repeated sections is generally better than 3 ppm (3×10^{-6} SI). Both tools are housed by non-magnetic materials; tools are logged at 600 m/h and the data are recorded every 5 cm.

Shore-Based Log Processing

Processing, quality control, and display of the logging data were performed at each of the seven holes logged during Leg 167 by the Borehole Research Group (BRG) at LDEO and the Institut Mediterraneen de Technologie, using Schlumberger "Logos" software and additional programs developed by members of the BRG. Displays of most of these processed data are available, with accompanying text, at the end of the appropriate site chapters and on CD-ROM, back pocket, this volume. Files of all processed logs (including FMS, dipmeter, temperature data, high-resolution density and neutron data, sonic waveforms, and magnetic data not shown in printed form) and explanatory text are included on the CD-ROM; a directory of the contents of the disk is found at the front of this volume.

Shore-based processing of data from each hole consisted of (1) depth adjustments of all logs to a common measurement below the sea floor; (2) corrections specific to certain tools; and (3) quality control and rejection of unrealistic values.

The depth-shifting procedure is based on an interactive, graphical depth-match program that allows the processor to visually correlate logs and define appropriate shifts. The reference log and the log to be adjusted in depth are displayed side-by-side on a screen, and ties connect the two at positions chosen by the user. The total gamma-ray curve from the NGT or HNGS tool run on each logging string was used in most cases to correlate the logging runs. In general, the reference curve is chosen on the basis of constant, low cable tension and high cable speed (tools run at faster speeds are less likely to stick and are less susceptible to data degradation caused by ship heave). Other factors, however, such as the length of the logged interval, presence of bottom hole assembly, and the statistical quality of the collected data (better statistics are obtained at lower logging speeds) are also considered in the selection. A list of the amount of differential depth shifts applied at each hole is available upon request to BRG-LDEO.

Specific tool corrections were performed on the gamma-ray data to account for changes in borehole size and for the composition of the drilling fluid.

Quality control was performed by cross-correlation of all logging data. If the data processor concluded that individual log measurements represented unrealistic values, the choices were to either discard the data outright and substitute the null value of "–999.25," or identify a specific depth interval containing suspect values that must be used with caution. The latter are noted in the text that accompanies all processed log displays. Quality control of the acoustic data was based on discarding any of the four independent transit time measurements that were negative or that fell outside a range of reasonable values selected by the processor.

In addition to the standard 15.24-cm sampling interval, bulk density and neutron data were recorded at a sampling interval of 2.54 and 5.08 cm, respectively. The enhanced bulk-density curve is the result of Schlumberger enhanced processing technique performed on the MAXIS system on board. In normal processing, short-spacing data are smoothed to match the long-spacing data; however, in enhanced processing this is reversed. In a situation where there is good contact between the HLDT pad and the borehole wall (low density correction), the results are improved because the short-spacing data have better vertical resolution.

Locally, some intervals of log data appeared unreliable (usually because of poor hole conditions) and were not processed. In general, a large (>12 in) and/or irregular borehole affects most recordings, particularly those that require eccentralization (HLDT/APS) and a good contact with the borehole wall. Hole deviation can also degrade the data; the FMS, for example, is not designed to be run in holes that are more than 10° off the vertical, as the tool weight might cause the caliper to close.

The Geological Magnetic Tool collected data at two different sampling intervals, the standard 0.1524 m interval and 0.0508 m. Both data sets are routinely depth shifted to the reference run and to the seafloor.

REFERENCES

Akiba, F., 1986. Middle Miocene to Quaternary diatom biostratigraphy in the Nankai trough and Japan trench, and modified lower Miocene through Quaternary diatom zones for middle-to-high latitudes of the North Pacific. *In* Kagami, H., Karig, D.E., Coulbourn, W.T., et al., *Init. Repts. DSDP,* 87: Washington (U.S. Govt. Printing Office), 393–481.

Archie, G.E., 1942. The electrical resistivity log as an aid in determining some reservoir characteristics. *J. Pet. Technol.,* 5:1–8.

ASTM, 1980. Standard method for laboratory determination of water (moisture) content of soil, rock and soil-aggregate mixtures. In *Annual Book of ASTM Standards:* Philadelphia (Am. Soc. Testing and Mater.).

Backman, J., Schneider, D.A., Rio, D., and Okada, H., 1990. Neogene low-latitude magnetostratigraphy from Site 710 and revised age estimates of Miocene nannofossil datum events. *In* Duncan, R.A., Backman, J., Peterson, L.C., et al., *Proc. ODP, Sci. Results,* 115: College Station, TX (Ocean Drilling Program), 271–276.

Backman, J., and Shackleton, N.J., 1983. Quantitative biochronology of Pliocene and early Pleistocene calcareous nannofossils from the Atlantic, Indian and Pacific oceans. *Mar. Micropaleontol.,* 8:141–170.

Baldauf, J.G., and Barron, J.A., 1991. Diatom biostratigraphy: Kerguelen Plateau and Prydz Bay regions of the Southern Ocean. *In* Barron, J., Larsen, B., et al., *Proc. ODP, Sci. Results,* 119: College Station, TX (Ocean Drilling Program), 547–598.

Barron, J.A., 1980. Lower Miocene to Quaternary diatom biostratigraphy of Leg 57, off Northeastern Japan, Deep Sea Drilling Project. *In* von Huene, R., Nasu, N., et al., *Init. Repts. DSDP,* 56, 57 (Pt. 2): Washington (U.S. Govt. Printing Office), 641–685.

Barron, J.A., 1992. Neogene diatom datum levels in the equatorial and North Pacific. *In* Ishizaki, K., and Saito, T. (Eds.), *The Centenary of Japanese Micropaleontology:* Tokyo (Terra Sci. Publ.), 413–425.

Barron, J.A., and Gladenkov, A.Y., 1995. Early Miocene to Pleistocene diatom stratigraphy of Leg 145. *In* Rea, D.K., Basov, I.A., Scholl, D.W., and Allan, J.F. (Eds.), *Proc. ODP, Sci. Results,* 145: College Station, TX (Ocean Drilling Program), 3–19.

Barron, J.A., and Keller, G., 1983. Paleotemperature oscillations in the middle and late Miocene of the northeastern Pacific. *Micropaleontology,* 29:150–181.

Berggren, W.A., Kent, D.V., Swisher, C.C., III, and Aubry, M.-P., 1995. A revised Cenozoic geochronology and chronostratigraphy. *In* Berggren, W.A., Kent, D.V., Aubry, M.-P., and Hardenbol, J. (Eds.), *Geochronology, Time Scales and Global Stratigraphic Correlation*. Spec. Publ.—Soc. Econ. Paleontol. Mineral., 54:129–212.

Berggren, W.A., Kent, D.V., and Flynn, J.J., 1985a. Jurassic to Paleogene, Part 2. Paleogene geochronology and chronostratigraphy. *In* Snelling, N.J. (Ed.), *The Chronology of the Geological Record.* Geol. Soc. London Mem., 10:141–195.

Berggren, W.A., Kent, D.V., and Van Couvering, J.A., 1985b. The Neogene, Part 2. Neogene geochronology and chronostratigraphy. *In* Snelling, N.J. (Ed.), *The Chronology of the Geological Record.* Geol. Soc. London Mem., 10:211–260.

Blow, W.H., 1969. Late middle Eocene to Recent planktonic foraminiferal biostratigraphy. *In* Brönnimann, P., and Renz, H.H. (Eds.), *Proc. First Int. Conf. Planktonic Microfossils, Geneva, 1967:* Leiden (E.J. Brill), 1:199–422.

Brassell, S.C., Eglinton, G., Marlowe, I.T., Pflaumann, U., and Sarnthein, M., 1986. Molecular stratigraphy: a new tool for climatic assessment. *Nature,* 320:129–133.

Cande, S.C., and Kent, D.V., 1992. A new geomagnetic polarity time scale for the Late Cretaceous and Cenozoic. *J. Geophys. Res.,* 97:13917–13951.

Cande, S.C., and Kent, D.V., 1995. Revised calibration of the geomagnetic polarity timescale for the Late Cretaceous and Cenozoic. *J. Geophys. Res.,* 100:6093–6095.

Caulet, J.-P., Nigrini, C., and Schneider, D.A., 1993. High resolution Pliocene–Pleistocene radiolarian stratigraphy of the tropical Indian Ocean. *Mar. Micropal.,* 22:111–129.

Ekstrom, M.P., Dahan, C.A., Chen, M.-Y., Lloyd, P.M., and Rossi, D.J., 1986. Formation imaging with microelectrical scanning arrays. *Trans. SPWLA 27th Annu. Logging Symp.,* Pap. BB.

Emeis, K.-C., and Kvenvolden, K.A., 1986. Shipboard organic geochemistry on *JOIDES Resolution. ODP Tech. Note,* 7.

Espitalié, J., Deroo, G., and Marquis, F., 1986. La pyrolyse Rock-Eval et ses applications, Partie III. *Rev. Inst. Fr. Pet.,* 41:73–89.

Fisher, A., and Becker, K., 1993. A guide to ODP tools for downhole measurements. *ODP Tech. Note,* 10.

Foreman, H.P., 1975. Radiolaria from the North Pacific, Deep Sea Drilling Project, Leg 32. *In* Larson, R.L., Moberly, R., et al., *Init. Repts. DSDP,* 32: Washington (U.S. Govt. Printing Office), 579–676.

Fornaciari, E., Raffi, I., Rio, D., Villa, G., Backman, J., and Olafsson, G., 1990. Quantitative distribution patterns of Oligocene and Miocene calcareous nannofossils from the western equatorial Indian Ocean. *In* Duncan, R.A., Backman, J., Peterson, L.C., et al., *Proc. ODP, Sci. Results,* 115: College Station, TX (Ocean Drilling Program), 237–254.

Gartner, S., 1992. Miocene nannofossil chronology in the North Atlantic, DSDP Site 608. *Mar. Micropaleontol.,* 18:307–331.

Gersonde, R., and Burckle, L.H., 1990. Neogene diatom biostratigraphy of ODP Leg 113, Weddell Sea (Antarctic Ocean). *In* Barker, P.F., Kennett, J.P., et al., *Proc. ODP, Sci. Results,* 113: College Station, TX (Ocean Drilling Program), 761–789.

Gieskes, J.M., Gamo, T., and Brumsack, H., 1991. Chemical methods for interstitial water analysis aboard *JOIDES Resolution. ODP Tech. Note,* 15.

Goldberg, D., 1990. Test performance of the Ocean Drilling Program wireline heave motion compensator. *Sci. Drill.,* 1:206–209.

Hagelberg, T., Shackleton, N., Pisias, N., and Shipboard Scientific Party, 1992. Development of composite depth sections for Sites 844 through 854. *In* Mayer, L., Pisias, N., Janecek, T., et al., *Proc. ODP, Init. Repts.,* 138 (Pt. 1): College Station, TX (Ocean Drilling Program), 79–85.

Harris, S., Hagelberg, T., Mix, A., Pisias, N., and Shackleton, N.J., 1995. Sediment depths determined by comparisons of GRAPE and logging density data during Leg 138. *In* Pisias, N.G., Mayer, L.A., Janecek, T.R., Palmer-Julson, A., and van Andel, T.H. (Eds.), *Proc. ODP, Sci. Results,* 138: College Station, TX (Ocean Drilling Program), 47–57.

Harwood, D.M., and Maruyama, T., 1992. Middle Eocene to Pleistocene diatom biostratigraphy of Southern Ocean sediments from the Kerguelen Plateau, Leg 120. *In* Wise, S.W., Jr., Schlich, R., et al., *Proc. ODP, Sci. Results,* 120: College Station, TX (Ocean Drilling Program), 683–733.

Hays, J.D., 1970. Stratigraphy and evolutionary trends of radiolaria in North Pacific deep sea sediments. *In* Hays, J.D. (Ed.), *Geological Investigations of the North Pacific.* Mem.—Geol. Soc. Am., 126:185–218.

Ingle, J.C., Jr., 1980. Cenozoic paleobathymetry and depositional history of selected sequences within the southern California continental borderland. *Spec. Publ. Cushman Found. Foraminiferal Res.,* 19:163–195.

Johnson, D.A., Schneider, D.A., Nigrini, C.A., Caulet, J.-P., and Kent, D.V., 1989. Pliocene-Pleistocene radiolarian events and magnetostratigraphic calibrations for the tropical Indian Ocean. *Mar. Micropaleontol.,* 14:33–66.

Kennett, J.P., Baldauf, J.G., and Lyle, M. (Eds.), 1995. *Proc. ODP, Sci. Results,* 146 (Pt. 2): College Station, TX (Ocean Drilling Program).

Kennett, J.P., and Srinivasan, M.S., 1983. *Neogene Planktonic Foraminifera: A Phylogenetic Atlas:* Stroudsburg, PA (Hutchinson Ross).

Koizumi, I., 1992. Diatom biostratigraphy of the Japan Sea: Leg 127. *In* Pisciotto, K.A., Ingle, J.C., Jr., von Breymann, M.T., Barron, J., et al., *Proc. ODP, Sci. Results,* 127/128 (Pt. 1): College Station, TX (Ocean Drilling Program), 249–289.

Koizumi, I., and Tanimura, Y., 1985. Neogene diatom biostratigraphy of the middle latitude western North Pacific, Deep Sea Drilling Project Leg 86. *In* Heath, G.R., Burckle, L.H., et al., *Init. Repts. DSDP,* 86: Washington (U.S. Govt. Printing Office), 269–300.

Lagoe, M.B., and Thompson, P.R., 1988. Chronostratigraphic significance of late Cenozoic planktonic foraminifera from the Ventura Basin, California: potential for improving tectonic and depositional interpretation. *J. Foraminiferal Res.,* 18:250–266.

Lazarus, D., Spencer-Cervato, C., Pianka-Biolzi, M., Beckmann, J.P., von Salis, K., Hilbrecht, H., and Thierstein, H., 1995. Revised chronology of Neogene DSDP holes from the world. *ODP Tech. Note,* 24.

Mazzullo, J.M., Meyer, A., and Kidd, R.B., 1988. New sediment classification scheme for the Ocean Drilling Program. *In* Mazzullo, J., and Graham, A.G. (Eds.), *Handbook for Shipboard Sedimentologists.* ODP Tech. Note, 8:45–67.

McKee, E.D., and Weir, G.W., 1953. Terminology for stratification and cross-stratification in sedimentary rocks. *Geol. Soc. Am. Bull.,* 64:381–390.

Merrill, R.B., and Beck, J.W., 1995. The ODP color digital imaging system: color logs of Quaternary sediments from the Santa Barbara Basin, Site 893. *In* Kennett, J.P., Baldauf, J.G., and Lyle, M. (Eds.), *Proc. ODP, Sci. Results,* 146 (Pt. 2): College Station, TX (Ocean Drilling Program), 45–59.

Moore, T.C., Jr., 1995. Radiolarian stratigraphy, Leg 138. *In* Pisias, N.G., Mayer, L.A., Janecek, T.R., Palmer-Julson, A., and van Andel, T.H. (Eds.), *Proc. ODP, Sci. Results,* 138: College Station, TX (Ocean Drilling Program), 191–232.

Morley, J.J., and Nigrini, C., 1995. Miocene to Pleistocene radiolarian biostratigraphy of North Pacific Sites 881, 884, 885, 886, and 887. *In* Rea, D.K., Basov, I.A., Scholl, D.W., and Allan, J.F. (Eds.), *Proc. ODP, Sci. Results,* 145: College Station, TX (Ocean Drilling Program), 55–91.

Nigrini, C., 1971. Radiolarian zones in the Quaternary of the equatorial Pacific Ocean. *In* Funnell, B.M., and Riedel, W.R. (Eds.), *The Microplaeontology of Oceans:* Cambridge (Cambridge Univ. Press), 443–461.

Okada, H., and Bukry, D., 1980. Supplementary modification and introduction of code numbers to the low-latitude coccolith biostratigraphic zonation (Bukry, 1973; 1975). *Mar. Micropaleontol.,* 5:321–325.

Olafsson, G., and Villa, G., 1992. Reliability of sphenoliths as zonal markers in Oligocene sediments from the Atlantic and Indian oceans. *In* Proto Decima, F., Monechi, S., and Rio, D. (Eds.), *Proc. Int. Nannoplankton Assoc. Conf., Firenze 1989.* Mem. Sci. Geol., 43:261–275.

Olafsson, G., 1991. Quantitative calcareous nannofossil biostratigraphy and biochronology of early through late Miocene sediments from DSDP Hole 608. *Medd. Stockholm Univ. Inst. Geol. Geochem.,* 203.

Peters, K.E., 1986. Guidelines for evaluating petroleum source rock using programmed pyrolysis. *AAPG Bull.,* 70:318–329.

Pozzi, J.-P., Martin, J.P., Pocachard, J., Feinberg, H., and Galdeano, A., 1988. In situ magnetostratigraphy: interpretation of magnetic logging in sediments. *Earth Planet. Sci. Lett.,* 88:357–373.

Prahl, F.G., Muehlhausen, L.A., and Zahnle, D.L., 1988. Further evaluation of long-chain alkenones as indicators of paleoceanographic conditions. *Geochim. Cosmochim. Acta,* 52:2303–2310.

Prahl, F.G., and Wakeham, S.G., 1987. Calibration of unsaturation patterns in long-chain ketone compositions for paleotemperature assessment. *Nature,* 330:367–369.

Prell, W.L., Niitsuma, N., et al., 1989. *Proc. ODP, Init. Repts.,* 117: College Station, TX (Ocean Drilling Program).

Raffi, I., Backman, J., Rio, D., and Shackleton, N.J., 1993. Plio-Pleistocene nannofossil biostratigraphy and calibration to oxygen isotopes stratigraphies from Deep Sea Drilling Project Site 607 and Ocean Drilling Program Site 677. *Paleoceanography,* 8:387–408.

Raffi, I., and Flores, J.-A., 1995. Pleistocene through Miocene calcareous nannofossils from eastern equatorial Pacific Ocean (Leg 138). *In* Pisias, N.G., Mayer, L.A., Janecek, T.R., Palmer-Julson, A., and van Andel, T.H. (Eds.), *Proc. ODP, Sci. Results,* 138: College Station, TX (Ocean Drilling Program), 233–286.

Riedel, W.R., and Sanfilippo, A., 1970. Radiolaria, Leg 4, Deep Sea Drilling Project. *In* Bader, R.G., Gerard, R.D., et al., *Init. Repts. DSDP,* 4: Washington (U.S. Govt. Printing Office), 503–575.

Riedel, W.R., and Sanfilippo, A., 1978. Stratigraphy and evolution of tropical Cenozoic radiolarians. *Micropaleontology,* 24:61–96.

Sanfilippo, A., Westberg-Smith, M.J., and Riedel, W.R., 1985. Cenozoic radiolaria. *In* Bolli, H.M., Saunders, J.B., and Perch-Nielsen, K. (Eds.), *Plankton Stratigraphy:* Cambridge (Cambridge Univ. Press), 631–712.

Shackleton, N.J., Baldauf, J.G., Flores, J.-A., Iwai, M., Moore, T.C. Jr., Raffi, I., and Vincent, E., 1995. Biostratigraphic summary for Leg 138. *In*

Pisias, N.G., Mayer, L.A., Janecek, T.R., Palmer-Julson, A., and van Andel, T.H. (Eds.) *Proc. ODP, Sci. Results*, 138: College Station, TX (Ocean Drilling Program), 517–536.
Shipboard Scientific Party, 1996. Explanatory notes. *In* Jansen, E., Raymo, M.E., Blum, P., et al., *Proc. ODP, Init. Repts.*, 162: College Station, TX (Ocean Drilling Program), 21–45.
Spencer-Cervato, C., Lazarus, D.B., Beckmann, J.-P., Von Salis Perch-Nielsen, K., and Biolzi, M., 1993. New calibration of Neogene radiolarian events in the North Pacific. *Mar. Micropaleontol.*, 21:261–293.
Thierstein, H.R., Geitzenauer, K., Molfino, B., and Shackleton, N.J., 1977. Global synchroneity of late Quaternary coccolith datum levels: validation by oxygen isotopes. *Geology*, 5:400–404.
Tissot, B.P., and Welte, D.H., 1984. *Petroleum Formation and Occurrence* (2nd ed.): Heidelberg (Springer-Verlag).
Wyszecki, G., and Stiles, W.S., 1982. *Color Science: Concepts and Methods, Quantitative Data and Formulae* (2nd ed.): New York (Wiley).

Ms 167IR-102